ESA Climate Change Initiative (CCI+)

Essential Climate Variable (ECV)

Greenland_Ice_Sheet_cci+ (GIS_cci+)

Product Validation and Intercomparison Report (PVIR)

Prime & Science Lead: Louise Sandberg Sørensen

DTU Space, Copenhagen, Denmark

Technical Officer: Anna Maria Trofaier

ESA ECSAT, Didcot, United Kingdom

Consortium: Asiaq Greenland Survey (ASIAQ)

DTU-Space, Department of Geodynamics (DTU-S)

DTU-Space, Department of Microwaves and Remote Sensing (DTU-N)

Danish Meteorological Institute (DMI)

ENVironmental Earth Observation IT GmbH (ENVEO)

Science [&] Technology AS (S&T)

Technische Universität Dresden (TUDr)

The Geological Survey of Denmark and Greenland (GEUS)

The Niels Bohr Institute (NBI)

Northumbria University (NU)

Signatures page

Prepared by	Anne Solgaard Lead Author, GEUS	
Issued by	Daniele Fantin, Project Manager, S[&]T	
Checked by	Louise Sørensen Science Leader, DTU-S	
Approved by	Anna Maria Trofaier ESA Technical Officer	

Table of Contents

Change Log

Issue	Author	Affected Section	Reason	Status
0.5	S&T	All	Document Creation	Created
1.0	ASIAQ	All	Reporting outcome of the validation performed	Delivered to ESA

Acronyms and Abbreviations

Acronyms	Explanation
ATBD	Algorithm Theoretical Basis Document
C3S	Copernicus Climate Change Service
CCI	Climate Change Initiative
CFL	Calving Front Location
CONAE	Comisión Nacional de Actividades Espaciales
CS2	CryoSat-2
CSR	Center for Space Research, University of Austin
DEM	Digital Elevation Model
(D)InSAR	(Differential) Interferometric Synthetic Aperture Radar
DL	Deep Learning
DMI	Danish Meteorological Institute
DTU-N	DTU Microwaves and Remote Sensing Group
DTU-S	DTU Geodynamics Group
E3UB	End-to-End ECV Uncertainty Budget
ECV	Essential Climate Variable
ENU	East North Up
ENVEO	ENVironmental Earth Observation IT GmbH
EO	Earth Observation
ESA	European Space Agency
GCOS	Global Climate Observation System
GCP	Ground Control Point
GEUS	Geological Survey of Denmark and Greenland

	Greenland_Ice_Sheet_cci+ Product Validation and Intercomparison Report (PVIR) for CCI+ Phase 2	Reference: DTU-ESA-GISCCI+-PVIR-002
greenland ice sheet cci		Version : 1.0 page
		Date : 16 December 2024 6/56

GFZ	Deutsche GeoForschungsZentrum
GIA	Glacial Isostatic Adjustment
GIS	Greenland Ice Sheet
GLL	Grounding Line Location
GMB	Gravimetry Mass Balance
GRACE(-FO)	The Gravity Recovery and Climate Experiment (Follow On)
IMBIE	Ice Sheet Mass Balance Inter-Comparison Exercise
InSAR	Interferometric Synthetic Aperture Radar
IPP	Interferometric Post-Processing
IV	Ice Velocity
JPL	NASA Jet Propulsion Laboratory
MAI	Multiple Aperture Interferometry
MEaSUREs	Making Earth System Data Records for Use in Research Environments (NASA)
MFID	Mass Flux and Ice Discharge
NBI	Niels Bohr Institute, University of Copenhagen
NEGIS	North East Greenland Ice Stream
NU	Northumbria University
OT	Offset Tracking
PROMICE	Danish Program for Monitoring of the Greenland Ice Sheet
RA	Radar Altimetry
RMS	Root Mean Square
S&T	Science and Technology AS
S2	Sentinel-2
SAR	Synthetic Aperture Radar

	Greenland_Ice_Sheet_cci+ Product Validation and Intercomparison Report (PVIR) for CCI+ Phase 2	Reference: DTU-ESA-GISCCI+-PVIR-002
		Version : 1.0 page
		Date : 16 December 2024 7/56

SEC	Surface Elevation Change
SLR	Satellite Laser Ranging
SMB	Surface Mass Balance
SOW	Statement of Work
TEC	Total Electron Content
TOA	Top of Atmosphere
TPROP	Technical Proposal
TUDr	Technische Universität Dresden
UL	University of Leeds
URD	User Requirement Document
TOPS	Terrain Observation by Progressive Scans

1 Introduction

1.1 Purpose and Scope

This document contains the Product Validation and Inter-comparison Report (PVIR) version 1 for the Greenland_Ice_Sheet_cci+ (GIS_cci+) project for CCI+ Phase 2, in accordance with contract and SoW [AD1 and AD2].

This document describes the results of the validation and intercomparison activities for each product as described in the Product Validation Plan for the Greenland_Ice_Sheet_cci (GIS_cci) project for CCI+ Phase 2 [RD1]. There are 4 products:

- Surface elevation Change (SEC and dSEC);
- Ice Velocity (IV);
- Gravimetry Mass Balance (GMB);
- Mass Flow Rate and Ice Discharge (MFID);

And one research object:

- Supraglacial Lakes (SGL)

The new prototype time-series 'Line-of-sight' product based on InSAR using Sentinel-1 data will not be validated as it is a prototype product and because no ground truth data exist. The validation of all data products is performed by ASIAQ and not by the partner producing the individual ECVs. Each partner responsible for an ECV has provided ASIAQ with the updated data product as well as the relevant validation data.

1.2 Document Structure

This document is structured as follows:

Chapter 1 contains an introduction to the document.

Chapter 2 – 6: A chapter for each ECV as well as the research object. The Surface Elevation chapter includes both SEC and dSEC. The IV chapter is split into radar IV including both offset tracking and InSAR based products, and optical IV. Each chapter is organised into the following sections:

- Sources of Independent validation data
- Validation procedure
- Validation procedure outcome
- Recommendations for improvements

Chapter 7 contains a reference list.

1.3 Applicable and Reference Documents

Table 1.1: List of Applicable Documents

No	Doc. Id	Doc. Title	Date	Issue/ Revision/ Version
AD1	ESA/Contract No. 4000126523/19/I-NB - Greenland_Ice-Sheets_CCI+ and its Appendix 1 (incl CCN3)	CCI+ Phase 1 New R&D pm CCI ECVs for Greenland _Ice Sheet_cci (incl CCN3)	Cont: 2019.03.06 CCN3: 2022.12.05	-

	Greenland_Ice_Sheet_cci+ Product Validation and Intercomparison Report (PVIR) for CCI+ Phase 2	Reference: DTU-ESA-GISCCI+-PVIR-002
		Version : 1.0 page
		Date : 16 December 2024 9/56

AD2	ESA-EOP-SC-AMT-2021-53	Climate Change Initiative Extension (CCI+) Phase 2 - New R&D on CCI Essential Climate Variables -SoW (incl Annexes)	2022.06.10	Issue 1 Revision 2
RD1	ST-DTU-ESA-GUCCI-PVP-001	ESA Climate Change Initiative (CCI+) Essential Climate Variable (ECV) Greenland_Ice_Sheet_cci+ (GIS_cci+) Product Validation Plan	2023.12.01	Version 3

2   Surface elevation change (SEC and dSEC)

The validation strategies for the SEC data products are described in section 6.1 of the "Product Validation Plan for the Ice_Sheets_cci project of ESA's Climate Change Initiative" [AD3], however the described round robin will be omitted. Hence, the main validations efforts will focus on:

- Comparison of temporally consistent airborne elevation changes with satellite altimeter elevation changes.
- Comparison of elevation changes derived from different sensors (e.g. radar vs. laser).

The SEC validation will be based upon the following metrics:
- RMSE (with respect to independent validation data)
- Temporal/spatial coverage and density of observations.

The dSEC validation will be based on time series intercomparisons, in selected points.
- RMSE

This chapter gives a complete report of the activities carried out to assess the quality of the SEC and dSEC products. In section 2.1 the sources of independent validation data considered for the SEC product validation, can be found, section 2.2 describes the validation procedure undertaken for the final SEC product, section 2.3 gives the results of the performed validation, before the recommendation for future improvements are described in section 2.4.

2.1   Sources and selection of independent validation data

The main source of validation data for the SEC-product is elevation change derived from repeat airborne laser scanning. Due to the significantly smaller horizontal and vertical errors associated with laser data compared to radar data (Brenner et al., 2007), the SEC trends are validated against elevation change trends derived from airborne laser-scanner data after being averaged at similar grid resolution as the SEC product.
Here, two different observational platforms and data products are used:

1. NASA's Operation IceBridge (Krabill, 2014) Airborne Topographic Mapper (ATM). The ATM data are acquired seasonally in the months April to June, and on a nearly yearly basis starting in 1993. The ATM instrument is mounted on-board an aircraft, usually the NASA DC-8 or P3-B, and typically flown at an altitude of 450 m. Given a 30-degree swath width, the laser pulses illuminate an approximately 250 m wide path on the ground. Each pulse has a footprint diameter of 1 to 3 m. The elevation change trends used in the validation are generated from the IceBridge ATM L1B Elevation and Return Strength (version 2) product (Krabill, 2010), and the surface elevation change is available at the National Snow and Ice Data center as a Level-4 data product.

2. DTU airborne laser scanning (ALS) conducted as part of the Programme for Monitoring of the Greenland Ice Sheet (PROMICE) or ESA's CryoSat Validation Experiment (CryoVEx) campaigns (Blair and Hofton, 2012; Geological Survey of Denmark and Greenland, 2015; Sørensen et al., 2018; Skourup, 2011). The DTU ALS system measures surface elevation measurements from scanning the surface in an approximately 200m wide swath, and surface elevation change has been derived from all available repeat flight paths. In contrast to the ATM dataset the ALS data also contain surface elevation change records from autumn campaigns.

An advantage of using airborne campaigns is that they most often are targeted at areas of the ice sheet which undergoes significant surface changes, both in time and space and thereby are multiple repeats available over especially the ice margin, where the largest SEC occurs and the radar altimeter observations are most challenged. Additionally, the long time series of airborne observations also ensures that we have a representative sampling over the more stable interior of the ice sheet.

2.1.1   Validation data errors and biases

Errors in airborne laser scanning arise from several sources, such as errors in the pitch, roll, and yaw of the aircraft and instrument, as well as multipath effects. The latter arises when the direct path of the signal is blocked, thus increasing the travel time of the respective laser pulse and decreasing the resulting elevation estimate. The effect of the aircraft inertial navigation system pitch cancels when averaging and smoothing the observations, while the roll induces a cross-track error. Krabill et al, (2002) considered

repeat ATM flights in 1993/1998 and 1994/1999 and found the effects to produce SEC errors up to 1 cm/yr. Atmospheric errors are on the same order of magnitude, and thus vertical errors are typically less than 10 cm.

The validation data uncertainty is also associated with errors from the surface roughness in the area in which the trend is derived, particularly along the ice margin where significant changes may occur within the 200 m distance used for overlapping trajectories. Furthermore, a low number of estimation points reduce the accuracy of the generated trend.

2.2   Validation procedure for SEC

As the validation data (ATM/ALS) and the SEC-product have different spatial resolution (250 x 250 m vs. 5 x 5 km), the first step in the validation procedure is to average the validation data at the native posting of the SEC posting. This is done by assessing the median value of observations within a given grid cell. Then this median value is subtracted from the radar SEC estimate, and the mean, median and standard deviation (STD) hereof are computed. So are the minimum and maximum differences. Most often, the median is more informative of the product performance, as both data sets are subject to outliers and the coarser resolution of radar-SEC product induces larger negative biases at outlet glaciers. The radar-SEC product consists of trends generated from combining all available ESA radar observations from 1992 to present and as five-year running means. The current 24 available SEC estimates are validated against the available validation data spanning the same time-windows. The region the ice sheet evaluated in each of the validation reports will differ from year to year due to differences in the flight paths from year to year of the airborne data. Figure 2-1 shows the spatial distribution of the available data from 2011 fights which approximately repeated the observations made in 2007.
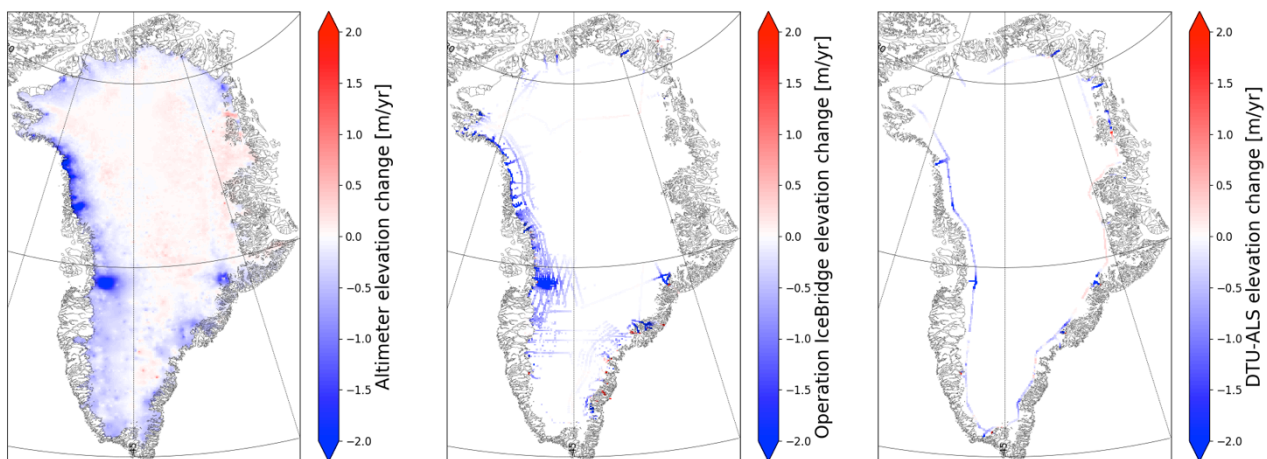

Figure 2-1: the spatial distribution of the available data from 2011 fights which approximately repeated the observations made in 2007

2.3   Validation procedure outcome for SEC

The combination of all available validation data (ATM/ALS) and the SEC-product produces a validation report for 19 of the 24 five-year running means in the SEC product, an example of the validation reports is shown in Figure 2-2. This report is typical for the time-slices but contains more data than the average example as both 2007 and 2011 had a lot of activity in Operation IceBridge and PROMICE. As observed with the different medians between the two validation data sets, the main bias between the airborne data and the SEC-product originates at the outlet glaciers. This may be attributed to slope-induced errors in radar data (Brenner et al. 1983; Roemer et al. 2007), which relocate the measurements up-slope from nadir and cause surface depressions such as the bottom of troughs and narrow valleys to be missed. The result is a very limited number of radar measurements inside the glacier trunks. Despite this, both the mean and STD are low relative to the min and max offsets, showing that radar data are indeed capable of resolving SEC even at the margin of the ice sheet.

	Greenland_Ice_Sheet_cci+ Product Validation and Intercomparison Report (PVIR) for CCI+ Phase 2	Reference: DTU-ESA-GISCCI+-PVIR-002
greenland ice sheet cci		Version : 1.0 page
		Date : 16 December 2024 12/56

	Operation IceBridge	DTU ALS	unit
number of data points	4411	1427	-
Mean difference	-0.28	-0.1	m pr. year
Median difference	-0.08	0.01	m pr. year
Standard deviation	0.88	0.67	m pr. year
Max. difference	6.84	5.55	m pr. year
Min. difference	-9.59	-7.82	m pr. year
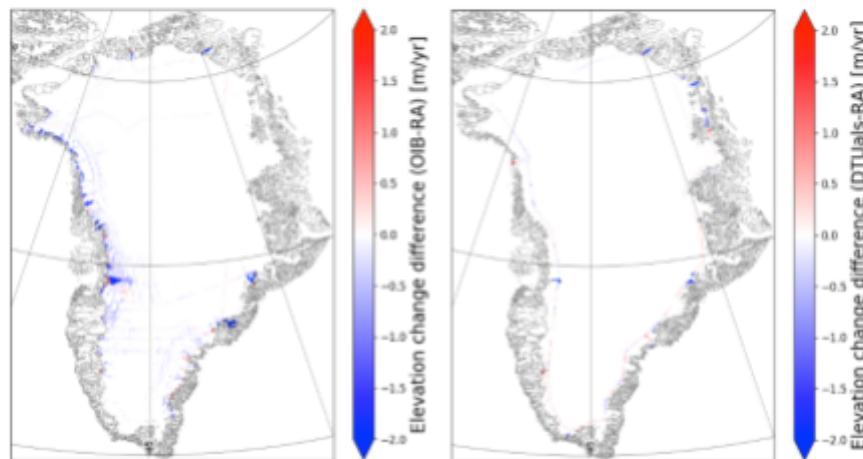
Figure 2-2: The validation with OIB and DTU ALS data. Top image is a table with the statistics from the validation and the lower image to the left is the OIB validation results and the lower image to the right is the DTU ALS validation results.

2.4 Validation procedure for dSEC

To validate the monthly surface elevation changes in the dSEC product, we compare with the ICESat-2 ATL15 data product (Smith et al., 2022). Both datasets are provided on grids and on compatible timescales, making such a comparison feasible.

For our analysis, we focus on four specific points located in the region surrounding Sermeq Kujalleq (commonly known as Jakobshavn Glacier). These points are carefully chosen to include locations both within and outside the ice stream, enabling an assessment of the dSEC product's ability to capture variations across different glacial environments. By including points on both inside the ice stream, where dynamic changes are expected to be significant, and outside, where changes are more subdued, we aim to gain an understanding of the product's performance under varying conditions.

It is important to note that the dSEC and ATL15 products are derived from different satellite sensors, each with distinct penetration depths and measurement characteristics. Therefore is it not expected that the two datasets will align perfectly. Instead, the aim of this validation is to assess the relative accuracy and reliability of the dSEC product while accounting for the inherent differences in sensor capabilities and measurement techniques.

2.5 Source and selection of independent validation data

For the dSEC the validation data used is ICESat-2 ATL15 gridded surface elevation change (Smith et al., 2022). The ATl15 product covers glaciers and ice sheet in the Arctic and Antarctic. It is derived from ICESat-2 data that uses the ATLAS instrument to acquire data.

The data is provided in a netCDF-4 format and covers the time period from 29 March 2019 to 23 March 2022.

The spatial reference system of the validation data is: WGS 84 / NSIDC Sea Ice Polar Stereographic North and EPSG:3413.

The data has a temporal resolution of 3 months. And the spatial resolution ranges from 1 km, 10 km, 20 km and 40 km grids. The data that is used for this validation in the 10 km grid.

2.6   Validation procedure outcome for dSEC

The results for the intercomparison can be seen below. The figures 2-3 show time series plots for four separate locations along a north-south transect along 48 degrees longitude. For each chosen point, the closest gridpoints from dSEC and ATL15 are compared. The compared grid cell points are found to be separated by a maximum of 1782.74 m and a minimum of 1269.54 m. This means that they all lie well within the 5x5km grid cells of the dSEC product. The dSEC product is shown in its native 1 month resolution and as three-month averages including errors (shaded areas) to be comparable with the ICESat-2 temporal resolution.

The RMSE between the timeseries ranges between 1.481 m and 2.604 m and is worst at the location 69.5,-48.0. The outcome is expected and the datasets lie approximately the same range, there are two key factors that most likely account for the majority of the differences between the two signals.
Firstly, the sensors are quite different, dSEC is from a Cryosat-2, which is a radar altimeter and ICESat-2 is a laser altimeter. This means that the sensors have differences in penetration depth and response to changes in surface characteristics which has a large impact on the scattering horizon and thus a direct impact on what "surface" the sensor measures. Despite this the datasets magnitude generally match well and the ICESat-2 data lies within the error margins of the dSEC product.

The different grid spacing most likely accounts for much of the difference in the intercomparison, as the signal is both spatially and temporally smoothed out the ICESat-2 signal compared to the dSEC product as the as the ICESat-2 data is averaged over a grid size of 10 km compared to the 5 km for the dSEC product.
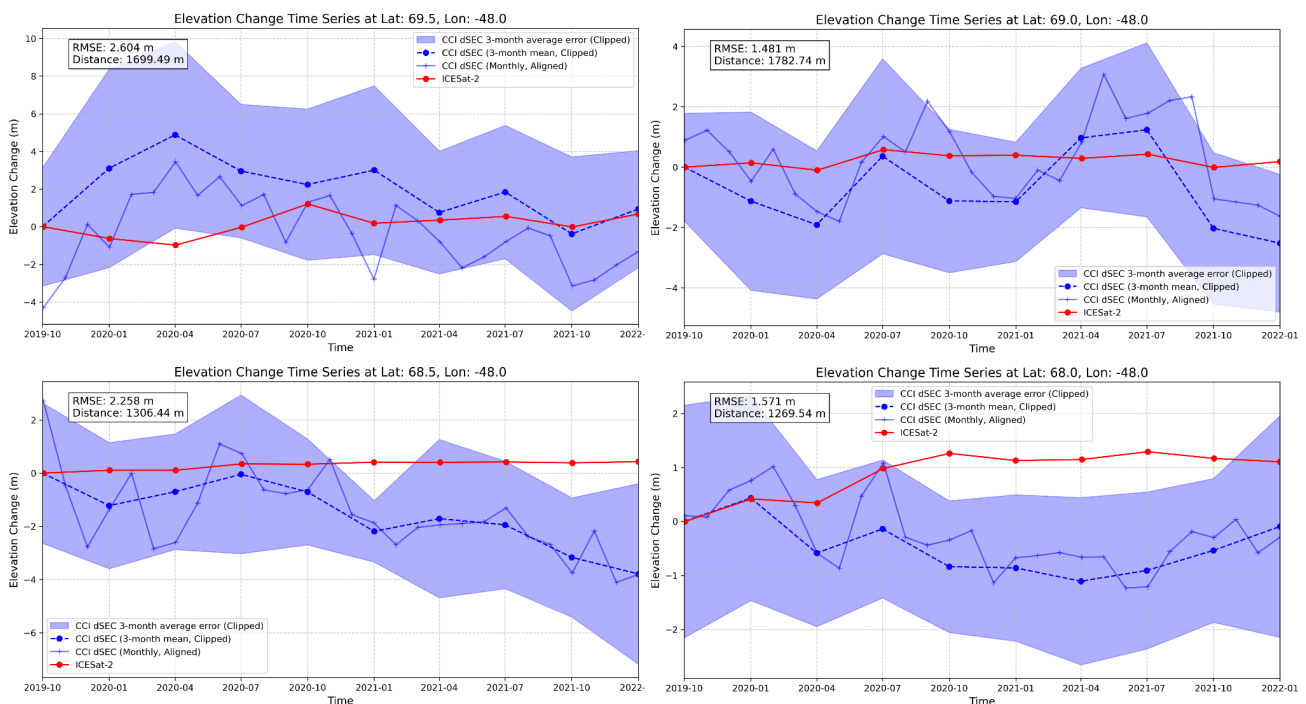

Figure 2-3, time series plots for dSEC and ICESat-2 data. Basic statistics are included in the legend including the distance between the two grid points plotted in each time series figure. The dashed line is the averaged dSEC data that fits with the same averaging window of the ICESat-2 data for better comparison.The blue shaded area is the averaged error over the 3 month smoothed dSEC data.

2.7 Recommendations for product improvements for both SEC and dSEC

One possibility for improving the SEC accuracy could be the use of a different retracker for the radar data. A number of studies have shown that such observations need to be adjusted for all three waveform parameters, i.e. the backscatter coefficient, leading edge width, and trailing edge slope, to ensure the highest accuracy (e.g. Khvorostovsky, 2012; Legresy et al, 2005, Simonsen and Sørensen 2017). However, as shown by Simonsen and Sørensen (2017) waveform corrections still leave a bias between the laser and radar estimated SEC, suggesting that a more surface-sensitive retracker could improve the laser-radar intercomparison. Further research is needed to derive true surface elevation change from radar altimetry, but the implementation of the shaper waveform in SAR and SARIn seems a promising technological advance in retrieving this goal (McMillan et al. 2019).

An improvement to the dSEC product would be to provide it at a range of spatial and temporal resolutions. This flexibility would enable more easy intercomparisons with the validation data across different scales and timeframes.

3   Ice Velocity (IV)

3.1   Radar IV

Here we describe the validation and quality assessment of the ice velocity products derived from Copernicus Sentinel-1 SAR data. Sentinel-1 provides continuous acquisitions of the Greenland Ice Sheet margins since October 2014. As part of the Greenland Ice Sheet CCI, ENVEO has generated an extensive archive of ice velocity products covering the entire mission duration. The ice velocity processing is ongoing and this document describes the validation efforts performed as part of Greenland Ice Sheet CCI Phase 2, extending the efforts performed in previous phases of the project.

3.1.1   Offset Tracking Product

The assessment is done for a subset of the individual OT track-by-track velocity maps (based on 12-day repeats) produced in the Greenland Ice Sheet CCI project and derived from Sentinel-1 (S1) SAR data. The individual track-by-track IV maps are the source data for the monthly and annually averaged mosaics. The quality assessment reported here include detailed intercomparisons, on a pixel-by-pixel basis, of the 12-day products against the Programme for Monitoring of the Greenland Ice Sheet (PROMICE; Solgaard et al., 2021) datasets and the CCI Optical IV estimates over three areas of interest. The product intercomparison provides a good level of quality assurance, where we report on the performance of the algorithm in stable terrain, i.e. where no velocity is expected. This provides a good overall indication of the bias introduced in the end-to-end velocity processing chain including co-registration of images, velocity retrieval, etc.

3.1.1.1   Sources and selection of independent validation data

For the product intercomparisons we use reference datasets from the PROMICE; (Solgaard et al., 2021) for the years 2022 and 2023, focusing on the key glaciers: Petermann (PTM), Jakobshavn (JH) and 79-Fjord. The PROMICE IV products are also derived from Sentinel-1 and available through the GEUS website. The datasets consist of composite maps averaged over 24 day periods. This differs from the products evaluated here, therefore an exact match is not to be expected. As a pre-processing step, the PROMICE IV maps were clipped and resampled to the same extent and 250 m grid spacing as the CCI datasets.

For the analysis of stable terrain, the moving ice is masked out using a polygon shapefile of the ice sheet and peripheral glacier outlines produced by Rastner et al (2012, updated 2018). The outlines are derived semi-automatically from Landsat-5 and Landsat-7 images, using a band ratio approach (red/SWIR) with scene specific thresholds and manual correction of debris cover, seasonal snow, shadow, water (outside of glaciers), sea ice and icebergs. By inverting the ice sheet/glacier shapefile and combining with an ocean mask a land mask file is created .

3.1.1.2   Validation procedure

We use different validation/intercomparison procedures; velocity product intercomparison and stable terrain analysis as outlined below:

1.   Stable terrain analysis: The results for the ice covered (moving) area are separated from ice-free (stable) ground. The masking is done using a polygon of the rock outlines. These data are then averaged over a whole year. The individual years are presented separately as individual velocity components in both a heat scatter plot and the histograms.

2.   PROMICE IV dataset for 2022 and 2023 used for product intercomparison on 250 m grids. We compare product data coverage, and generate statistics for both easting (x in plots) and northing (y in plots) velocity components as well as magnitude. These are presented in scatter plots and statistical time series for each location and pair. The pairs are stacked and combined in a single yearly comparison for each individual velocity component is computed pixel-by-pixel and compared between the product and the validation data in scatter plots.

3.1.1.3   Validation procedure outcome

In order to generate a more synoptic validation, the data from the individual geotifs has been averaged over every year for each location (and track) and the previously described analysis carried out (scatterplot, incl. statistics time series). Even though the same mask is used to generate the individual geotifs, there are variations in the coverage of datapoints. The faulty files have been excluded from this analysis.

Figure 3-1 presents the results of the stable terrain test as scatterplots of easting versus northing velocity components for all locations, split between 2022 and 2023. Figure3-2 shows the corresponding histograms of each location for both years. All data points from the individual image pairs are averaged in the plot. For Petermann the two tracks are presented separately. All the test regions are centered around 0 and all have an annual mean of <1 cm/d and a RMSE of <2 cm/d.
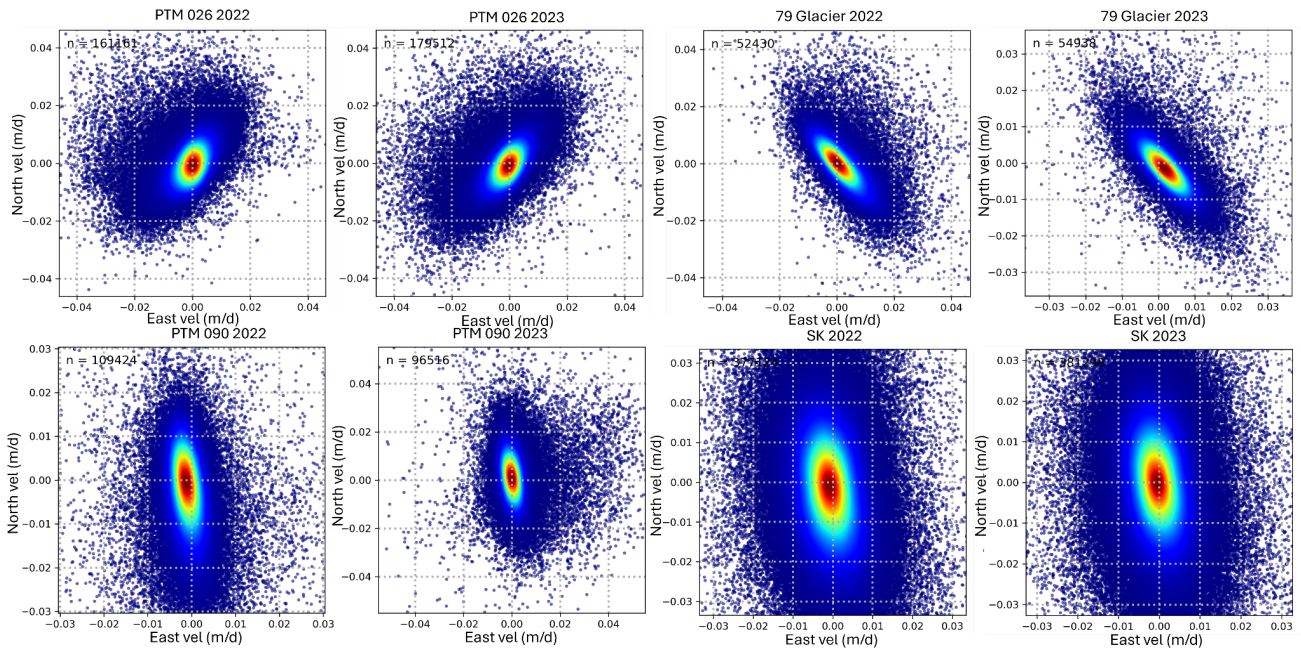
Figure 3-1: Results of the stable rock test for the different CCI+ velocity products. The scatter plots show easting velocity versus northing velocity with colour coding blue to red indicating point density from low to high. Both years of data are displayed 2022 and 2023.
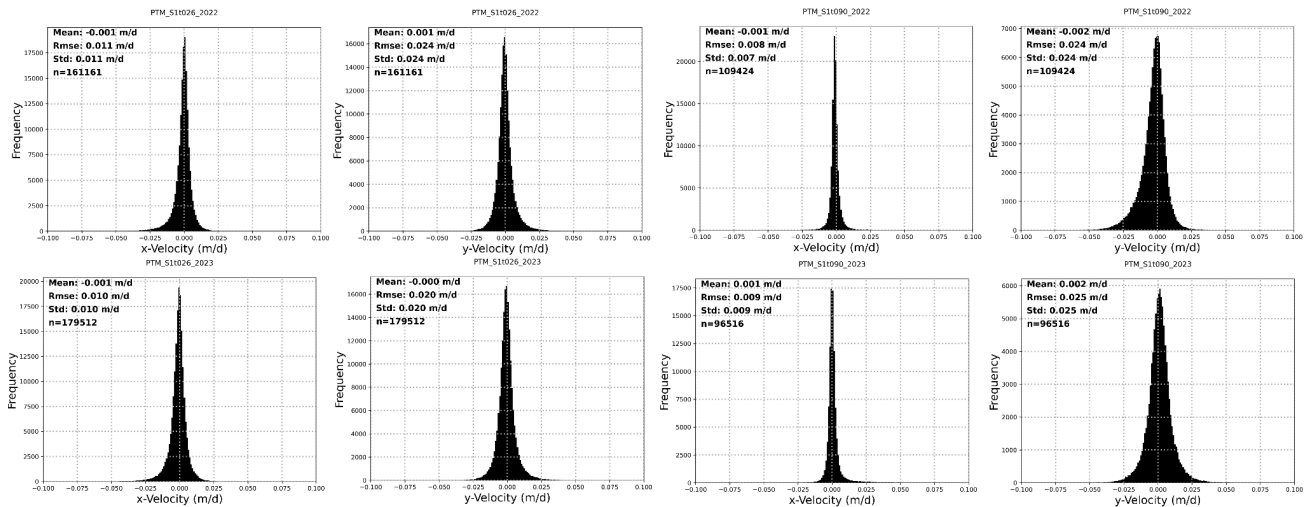
Figure 3-2: Histograms of the stable rock test. They are broken down into the easting and northing components for each location, for each year.
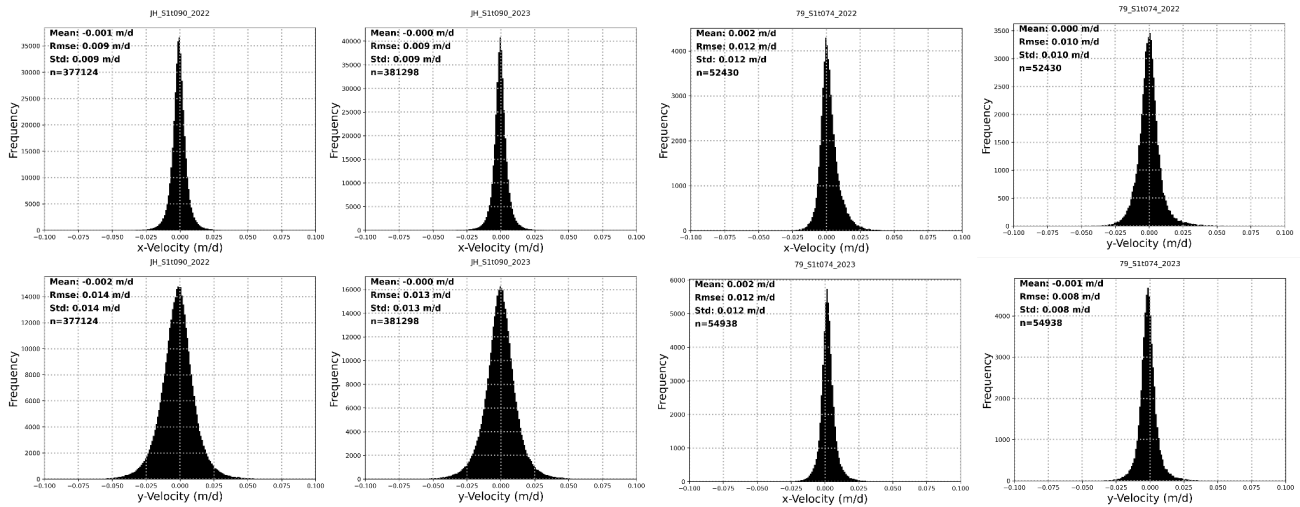

Figure 3-2 (Continued): Histograms of the stable rock test. They are broken down into the easting and northing components for each location, for each year.

The comparison of the individual velocity pairs show good agreement as displayed in both the magnitude statistics in figure 3-3 and the yearly scatter plots in figure 3-5 for the individual velocity components. In all cases for the individual plots the standard deviation of the velocity difference between the PROMICE dataset and the CCI dataset does not exceed higher than 0.2 m/d in all but two of the individual pairs.

In all examples there is a clear seasonal pattern of the data that corresponds to the number of pixels available for the intercomparison. Generally between May and October the number of available data points drops significantly. This is most likely due to the rapidly changing surface both in the form of melting in the spring transition and the snowfall arriving in autumn. This is also reflected in the standard deviation of the data in which pairs with good coverage have a lower standard deviation, and reduction in the number of points removed through filtering. The exception occurs in the key transition periods in spring and late autumn which is most likely a result of heavy significant melting in spring and snowfall in autumn. This pattern is reflected at all sites although the two sites furthest north, Nioghalvfjerds and Pertermann have a noticeably shorter period with lower data coverage than Sermeq Kujalleq.

The data density over the entire year varies for each location and appears to be linked to surface changes caused by both higher velocity areas and melt/snowfall. Figure 3-4 highlights this further where the medium- fast flow areas of the outlet glaciers correspond with areas that have lowest data density throughout the year. This is particularly apparent for Sermeq Kujalleq and Nioghalvfjerds glacier, however the fast flow areas at both sites are captured in most of the individual pairs, but the upstream fast flow areas have the lowest data coverage over the year. At Petermann the coverage is generally highest compared to the other two sites where most of the area has a temporal coverage of over half the individual pairs for both years and tracks, but coverage is better for track 026 than 090. In all cases coverage of individual pair data is better in 2022 than 2023.

This disparity in both spatial and temporal data coverage is particularly important for the generation of annual velocity products which need to take into consideration the significant spatio-temporal biases presented in figures 3-3 and 3-4.

Figure 3-5 shows all the stacked data of each individual velocity pair and the product estimate is plotted against the validation estimate. This is done for each individual velocity component and for each year. The agreement between the two datasets is very good and generally follows a 1-to-1 agreement at all sites.

|	greenland ice sheet cci	Greenland_Ice_Sheet_cci+ Product Validation and Intercomparison Report (PVIR) for CCI+ Phase 2	Reference: DTU-ESA-GISCCI+-PVIR-002
			Version : 1.0 page
			Date : 16 December 2024 18/56

Figure 3-3 : Results of individual pair comparison for each location for two years. The upper plot shows the standard deviation of the velocity difference over each pair for both the masked and unmasked data. We have only included one of the tracks for the Petermann as they both show a very similar result. We therefore only include track 026 as it has better spatial coverage.
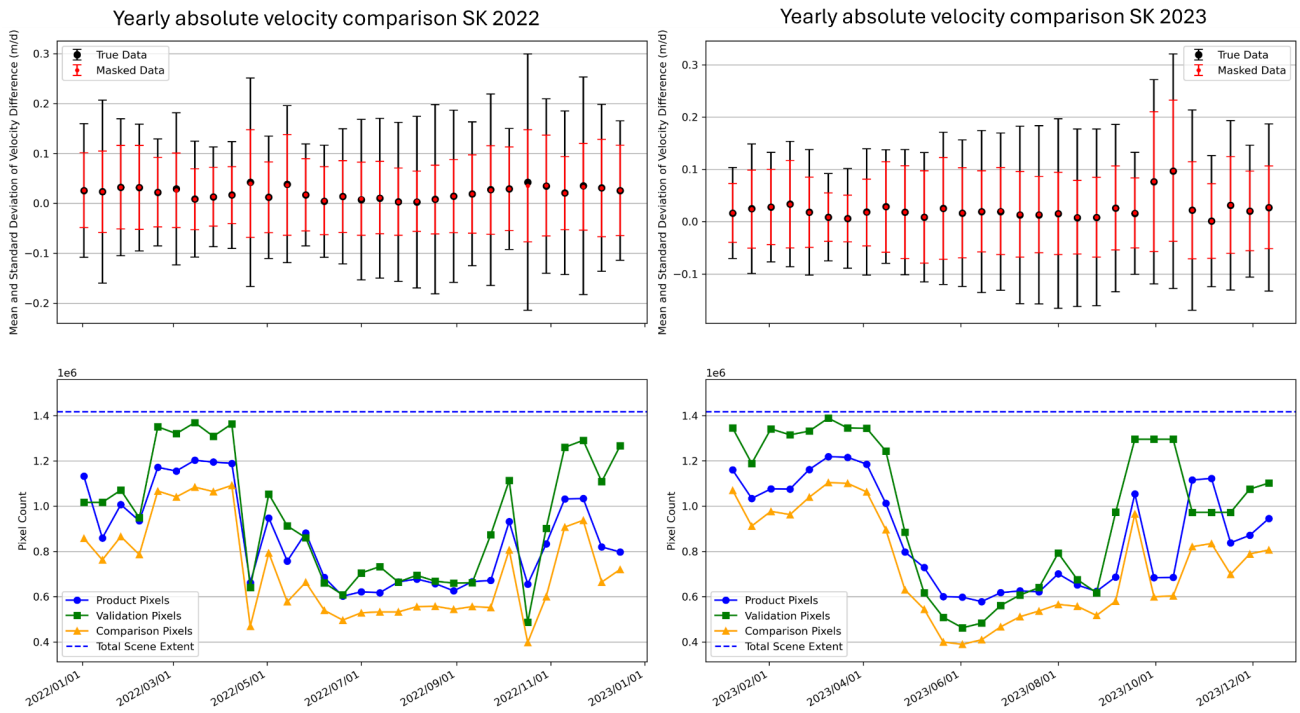
Figure 3-3 (continued): Results of individual pair comparison for each location for two years. The upper plot shows the standard deviation of the velocity difference over each pair for both the masked and unmasked data. We have only included one of the tracks for the Petermann as they both show a very similar result. We therefore only include track 026 as it has better spatial coverage.

	Greenland_Ice_Sheet_cci+ Product Validation and Intercomparison Report (PVIR) for CCI+ Phase 2	Reference: DTU-ESA-GISCCI+-PVIR-002 Version : 1.0 page Date : 16 December 2024 20/56

greenland
ice sheet
cci
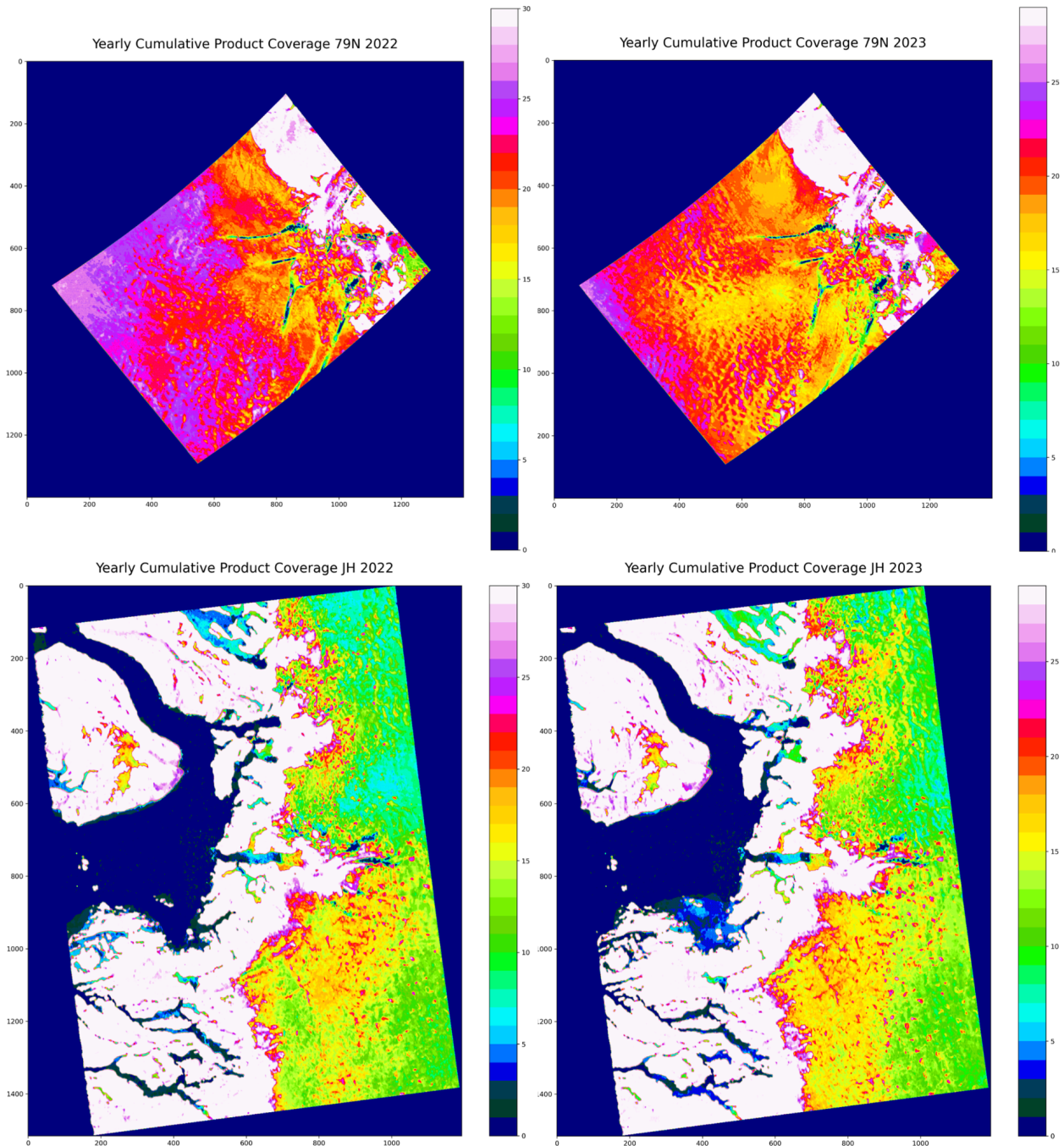
Figure 3-4: Spatiotemporal coverage of the datasets that show the data density over the three regions. The colour bar corresponds to the number of individual velocity estimates that have data in a given pixel. The maximum number of individual pairs per year was 30.
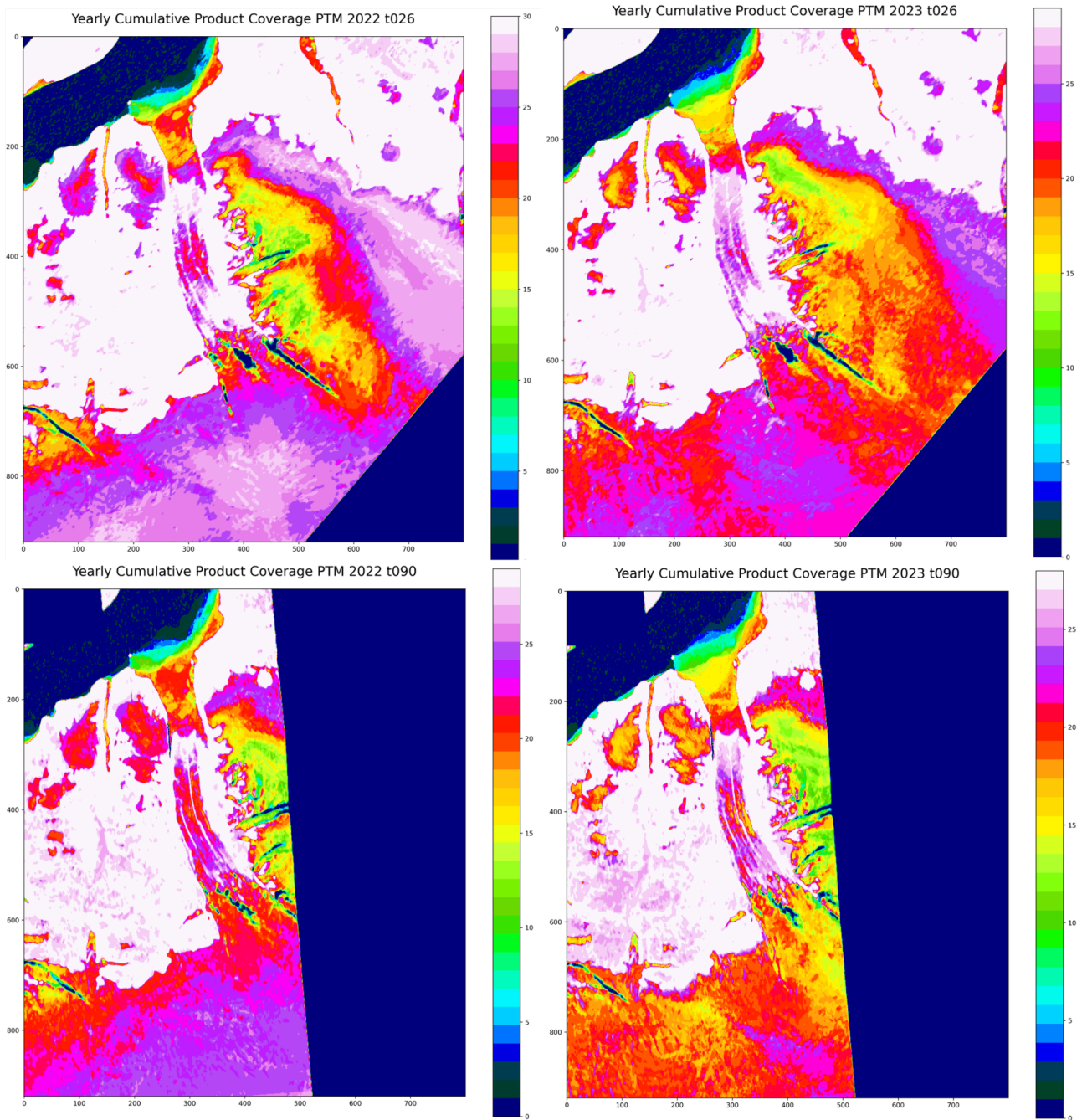
Figure 3-4 (Continued): Spatiotemporal coverage of the datasets that show the data density over the three regions. The colour bar corresponds to the number of individual velocity estimates that have data in a given pixel. The maximum number of individual pairs per year was 30.
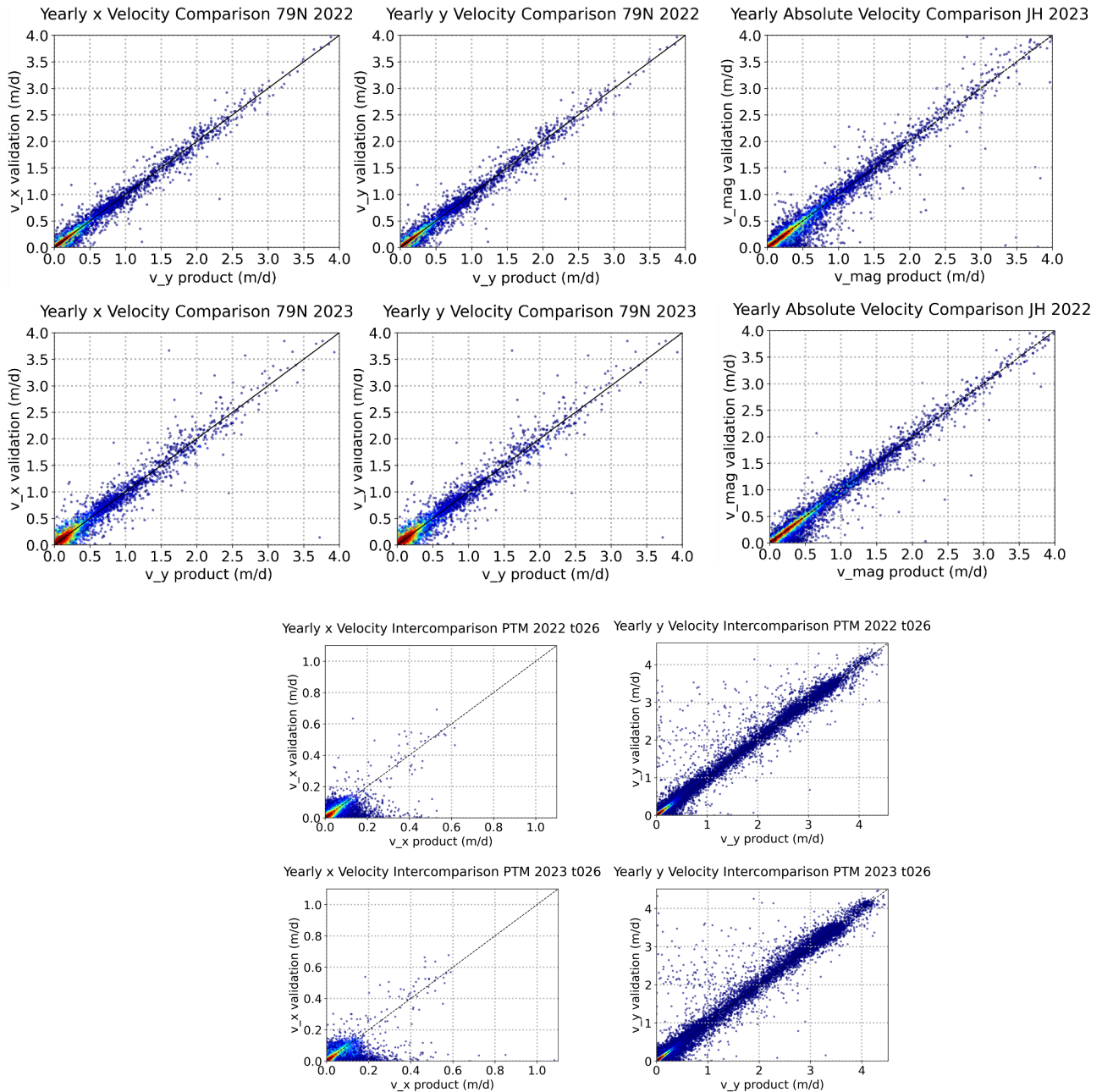
Figure 3-5: Yearly stacked pixel-by-pixel analysis between the product and the validation for each velocity component for each location. Note that for Petermann track 026 only.

3.1.1.4   Recommendations for products improvement

The assessment provided above indicates that the current IV products perform very well. The accuracy requirements for IV as described in the User Requirements Document (URD) of the Ice Sheets CCI project (Hvidberg, et al, 2012), identified through an extensive user survey within the glaciology community, lists a minimum accuracy of 30-100 m/y (0.08-0.27 m/d) with an optimum accuracy of 10-30 m/y (0.03-0.08 m/d). The results of our quality assessments fall well within this range. A key product improvement for IV is the InSAR processing developed within the GIS CCI+ Phase 1 project. The InSAR product significantly improves the accuracy of

the ice velocity, in particular in slower moving terrain. In the current project further work was performed on extending the application of the InSAR processing by including SAOCOM L-band SAR data for selected test regions.

Further enhancements performed during this phase of the project, but not yet included in the ice velocity products assessed here, is an adaptation of the offset tracking processing line which improves the amount of successful correlation matches in regions with very fast flow. This adaptation was necessary due to the failure of Sentinel-1B, reducing the repeat pass period of the mission from 6 to 12 days. It was found that the longer repeat pass period led to gaps in the ice velocity fields on very fast glaciers. By specifying a preset correlation window offset, based on a long-term averaged ice flow velocity map derived from Sentinel-1, the number of successful matches could be increased significantly, leading to less gaps in the ice velocity maps.

A further recommendation for improvement for the ice velocity product is to use the new Sentinel-1 Extended Timing Annotation Dataset (ETAD) product. ETAD was developed in a joint effort by the German Aerospace Center (DLR) and ESA and has been provided with the regular Sentinel-1 product since September 2023. The ETAD product provides a timing correction of the S-1 SAR products, that are based on modelling and ancillary data. It corrects for the tropospheric and ionospheric path delays, the tidal-based surface displacements (solid-earth tide), and SAR processing effects. The correction can enhance the absolute geolocation accuracy of the SAR images and the relative collocation accuracy of repeat pass image stacks which can improve the ice velocity estimation.

3.1.1.5   Acknowledgments of data contributors for IV validation

Data from the Programme for Monitoring of the Greenland Ice Sheet (PROMICE) and the Greenland Analogue Project (GAP) were provided by the Geological Survey of Denmark and Greenland (GEUS) at http://www.promice.dk.

3.2 Optical IV

3.2.1 Sources and selection of independent validation data

In order to validate the Sentinel-2 based optical IV products both in situ data and IV derived from other EO sources were considered. The main source of in situ data is the GPS data gathered by the PROMICE weather stations, however these stations are located on the ice sheet or relatively slow-moving ice rather than on the fast-flowing outlet glaciers. Since the optical IV products are focussed on the fast-flowing outlet glaciers, relevant in situ data is not available to our knowledge. The main alternative EO data source to derive IV from are SAR measurements. Both PROMICE and ENVEO have produced SAR based products from Sentinel-1 with good spatial temporal coverage allowing for a comparison with the Sentinel-2 optical based IV. Therefore, the two main sources that were selected for an independent validation are:

1) PROMICE Sentinel-1 (SAR) based IV
2) ENVEO Sentinel-1 (SAR) based IV

3.2.2 Validation procedure

For the validation it was decided to compare seasonal products because these products could be derived for all three IV datasets. A weighted seasonal product from ENVEO and PROMICE datasets was generated to match the time span of the Optical IV seasonal product. This approach was decided upon to take into consideration the data availability in each of the ENVEO/ PROMICE products.

The resulting datasets are of varying coverage (see figures 3.6-3.15), depending on the time span, location and the year. In general, the data coverage for the year 2023 is significantly worse than for 2022. This is also reflected in the number of days over which the seasonal product is calculated, which includes nearly double the number of days in 2022 compared to 2023.

Location	Year	Product Timespan	Number of days
Sermeq Kujalleq (JH)	2022	01.05.2022 – 27.08.2022	119
Sermeq Kujalleq (JH)	2023	24.05.2023 – 07.08.2023	75
Petermann Glacier (PTM)	2022	02.05.2022 – 29.08.2022	120
Petermann Glacier (PTM)	2023	06.07.2023 – 30.08.2023	56

Table 3-1 Based on the available data for all sources, the following seasonal products were used

The three different IV datasets (S&T, ENVEO and PROMICE) come at different resolutions and grids. To allow for a direct comparison the S&T and PROMICE datasets were re-gridded to 250m resolution to match the resolution and grid of the ENVEO dataset. We generate difference maps for both velocity components as well as the velocity magnitude and the corresponding histograms. For all of those the validation data are subtracted from the product. This is done for all locations and both years. Additionally, at Petermann two separate tracks were provided by ENVEO (track 090 and 026).

In all instances, differences larger than 1 m have been disregarded in the visual comparison. However, the statistics for both the whole dataset and the data clipped to 1 m difference have been calculated and are displayed in the histograms (figures 3.6-3.15).

As an ice mask had already been applied to the product before validation, no stable ground assessment was made for this product.

3.2.3   Validation procedure Outcome

The overall trend in IV is similar to the one observed in the SAR based products of both ENVEO and PROMICE (see figure Figure 3-6). In regions of low ice flow velocity, typically speeds are higher in the optical product. This is likely due to the limitations within the co-registration process. Furthermore, it should be noted that post processing steps, such as interpolation, smoothing and filtering, likely vary for the different datasets

We split the validation outcome into two sections based on the two locations, firstly we present the intercomparison of the three datasets for Sermeq Kujalleq for both 2022 and 2023. The 2022 intercomparison is generally very good with a narrow distribution and mean of 0.7 (ENVEO) and 0.9 (PROMICE) for the magnitude. The coverage is generally good in 2022 and thus allowing for a good comparison.
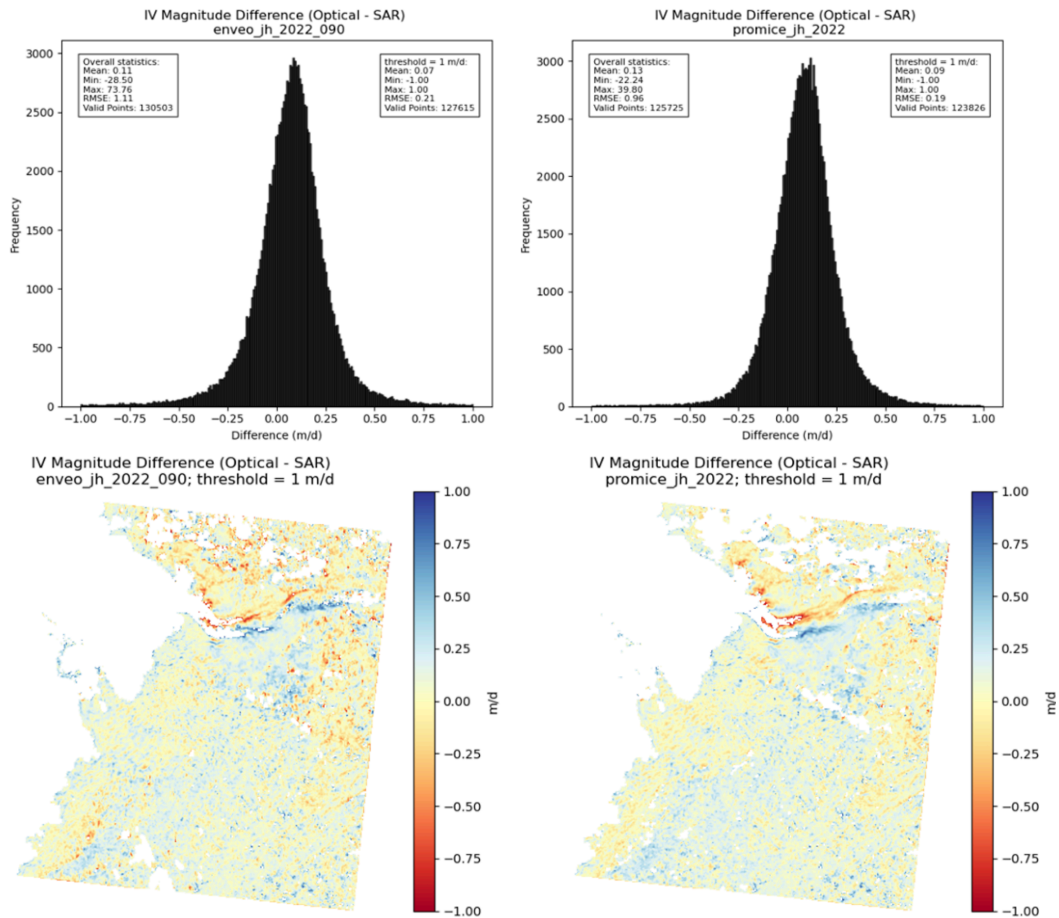
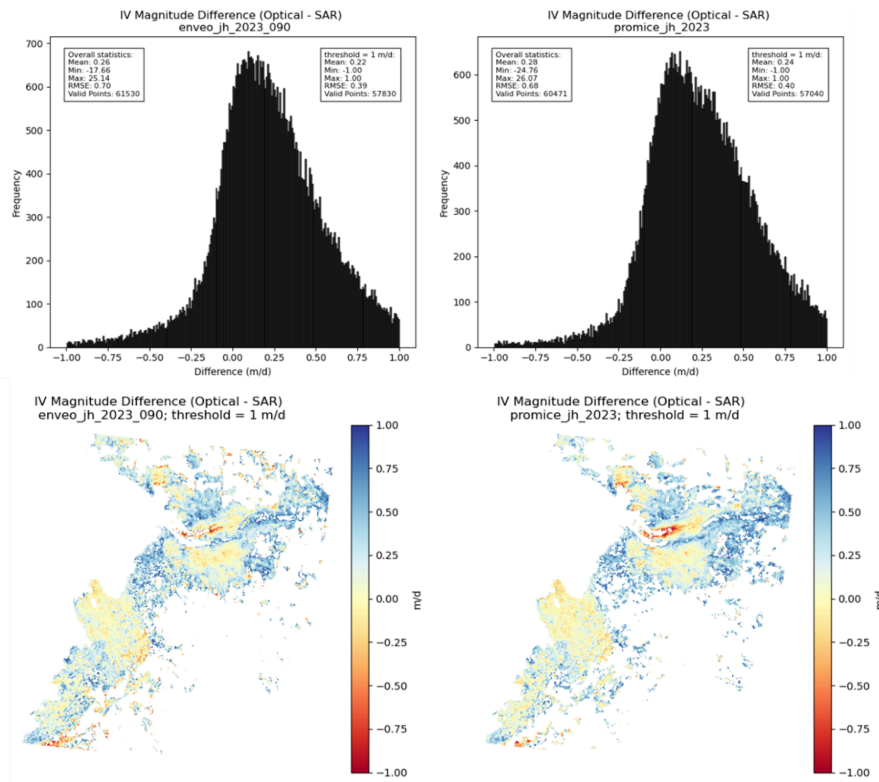*Figure 3-6 Sermeq Kujalleq (Jakobshavn Isbræ) magnitude intercomparison with ENVEO and PROMICE 2022 (see table 3-1 for exact time span of seasonal product).*
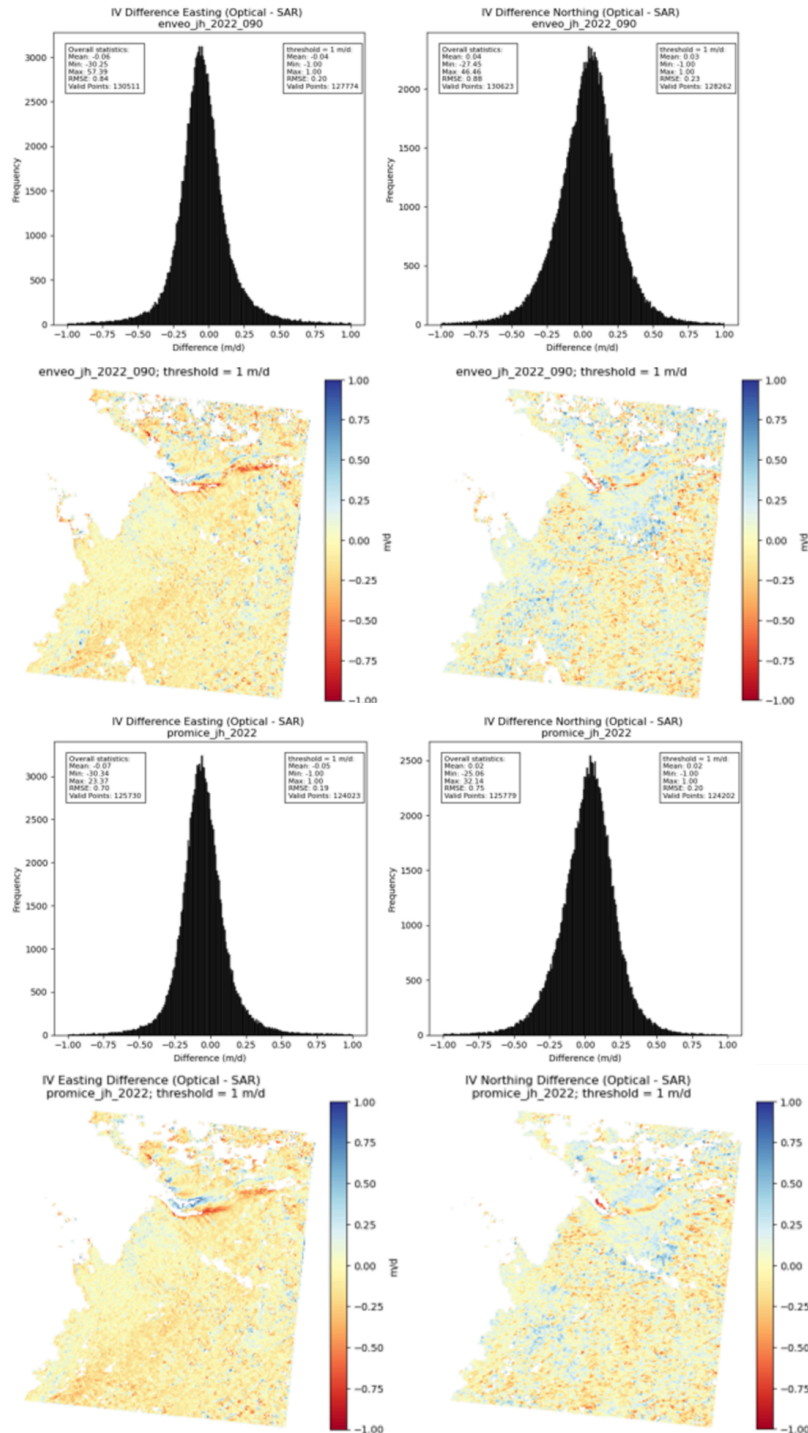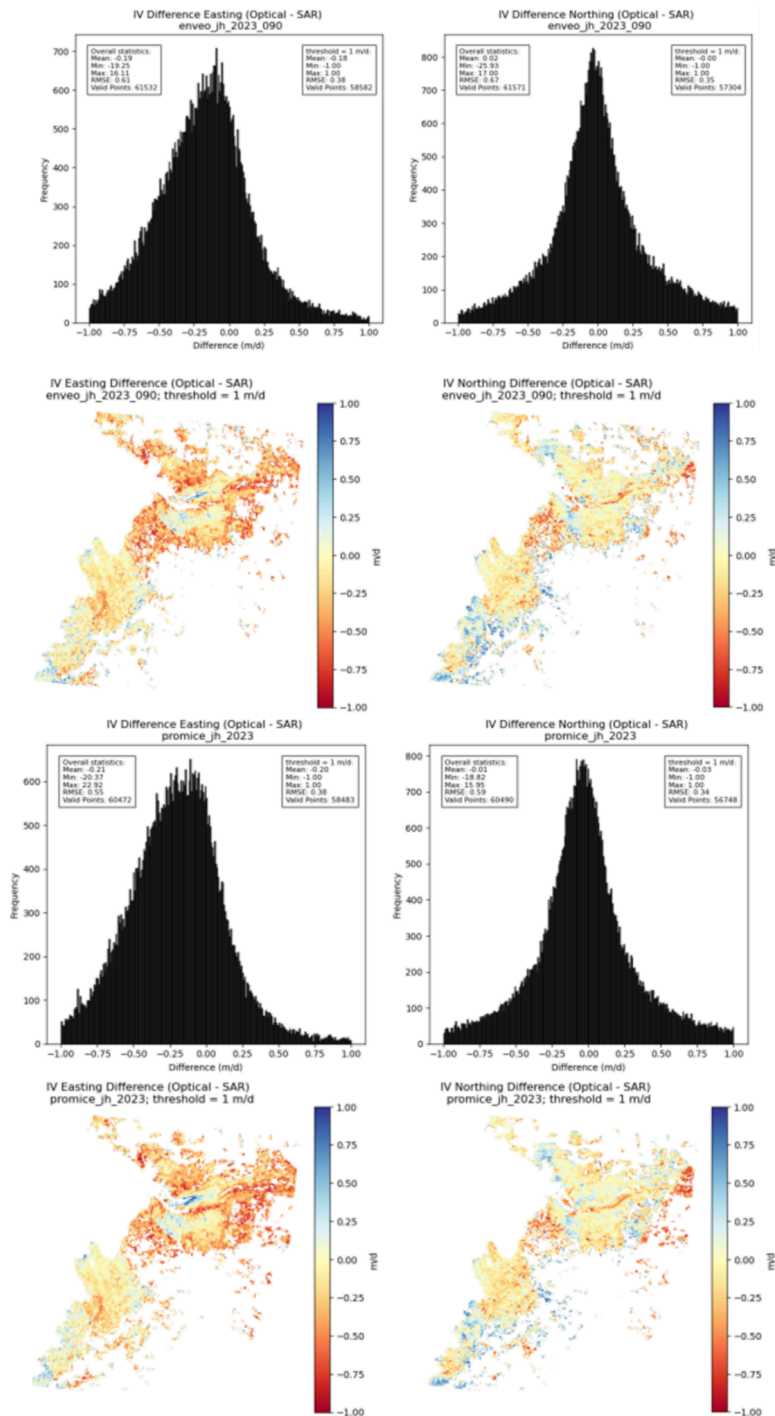
Figure 3-7 Sermeq Kujalleq (Jakobshavn Isbræ) easting and northing component intercomparison with ENVEO and PROMICE 2022 (see table 3-1 for exact time span of seasonal product).

Some slight discrepancies occur around the fast flow area in the individual velocity components that could reflect geolocation errors between the different datasets. The data indicates a slightly larger bias in the easting compared to the northing in 2022.

The data set has a very poor coverage in 2023 which could indicate a higher frequency of clouds in the scenes that significantly reduce the data coverage for the optical IV compared to that of the SAR. This is reflected in the number of comparison pixels. Approximately only half of the number of comparable pixels are available in 2023 compared to 2022. The pattern of offset remains consistent with a general overestimation of the optical IV compared to the two SAR products. However the area where the optical data consistently underestimates the velocity compared to the SAR products is in the very fast flowing outlet where the optical IV underestimates in both 2022 and 2023.

Figure 3-8 Sermeq Kujalleq (Jakobshavn Isbræ) magnitude intercomparison with ENVEO and PROMICE 2023 during the main melt season (see table 3-1 for exact time span of seasonal product).

Figure 3-9 Sermeq Kujalleq (Jakobshavn Isbræ) easting and northing component intercomparison with ENVEO and PROMICE 2023 (see table 3-1 for exact time span of seasonal product).

The second intercomparison site was Petermann glacier in the far north of Greenland. Here we present the velocity intercomparison for 2022 and 2023 .

In general the pattern of offset between the optical IV and the two SAR IV estimates is a very similar story to that found at Sermeq Kujalleq. In general the product intercomparison is very good with represented by very centred, normally distributed and tight histograms in both the magnitude and the individual velocity components. Here the coverage in the main outlet is much better than at Sermeq Kujalleq but this is likely a reflection of the slower ice velocity at Petermann. This is especially true for 2022, where 2023 has generally poorer coverage and is almost solely limited to the main outlet, with no significant coverage upstream or to the Eastern margin of the outlet. The poor coverage at both Sermeq Kujalleq and Pertermann glacier suggests that the cloud cover in 2023 was consistently higher than that in 2022 in both areas of Greenland

The trend of overestimation by the optical IV is more apparent in the 2023 estimates, and is particularly pronounced in the northing component compared to both the ENVEO and PROMICE datasets. Conversely, there seems to be a slight underestimation in the easting velocity component in 2023. Neither of these signals are very apparent in the velocity components in 2022.
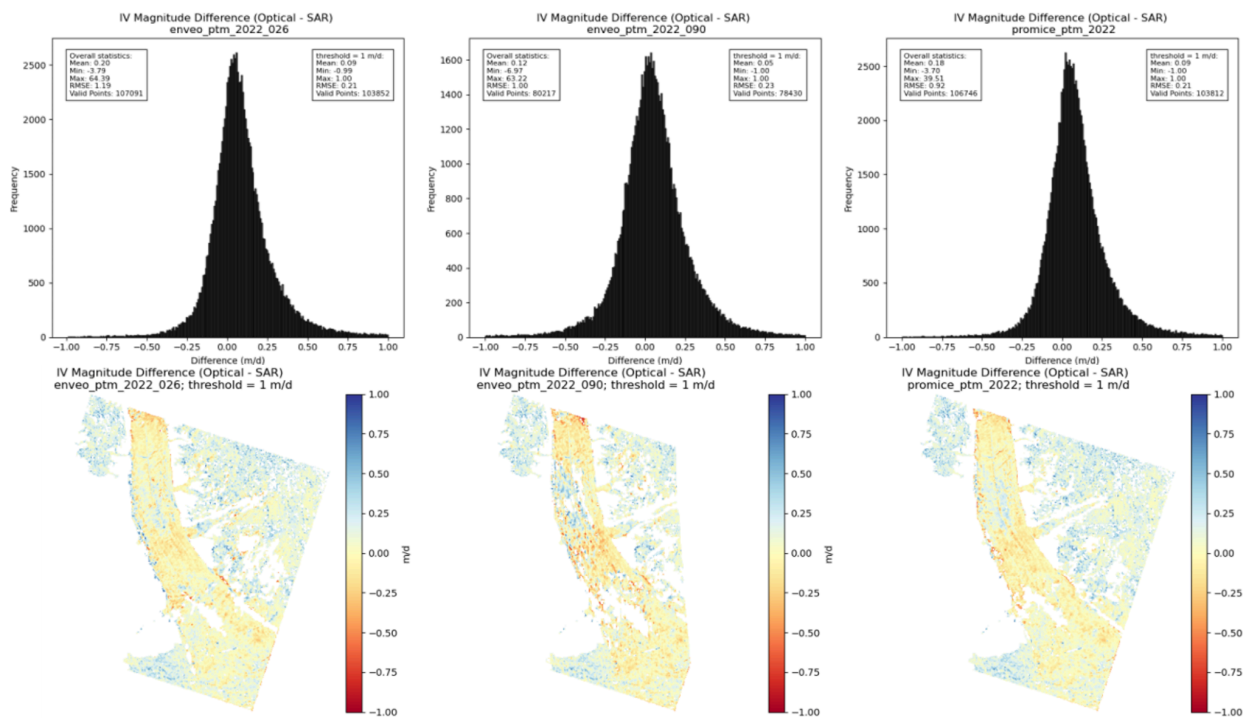
Figure 3-10 Petermann glacier magnitude intercomparison with ENVEO and PROMICE 2022 (see table 3-1 for exact time span of seasonal product).
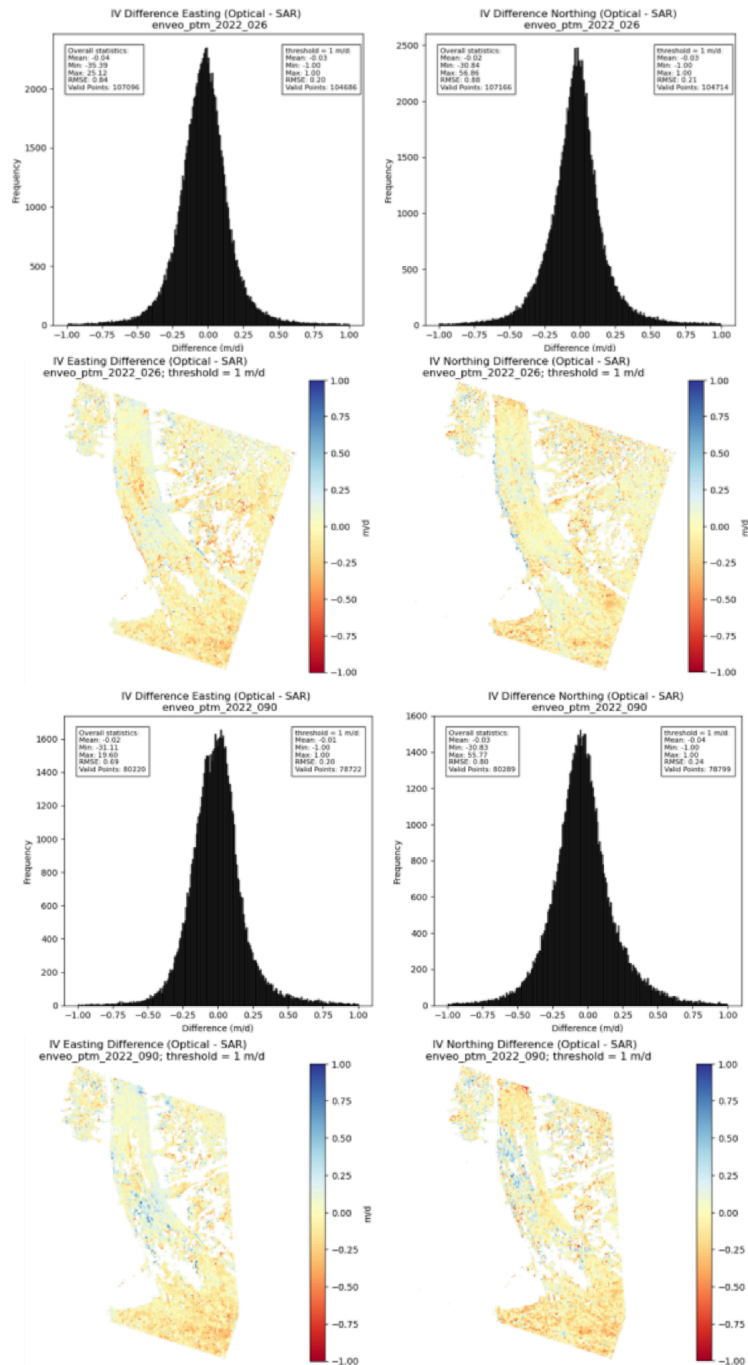
Figure 3-11 Petermann glacier easting and northing component intercomparison with ENVEO 2022. (see table 3-1 for exact time span of seasonal product).
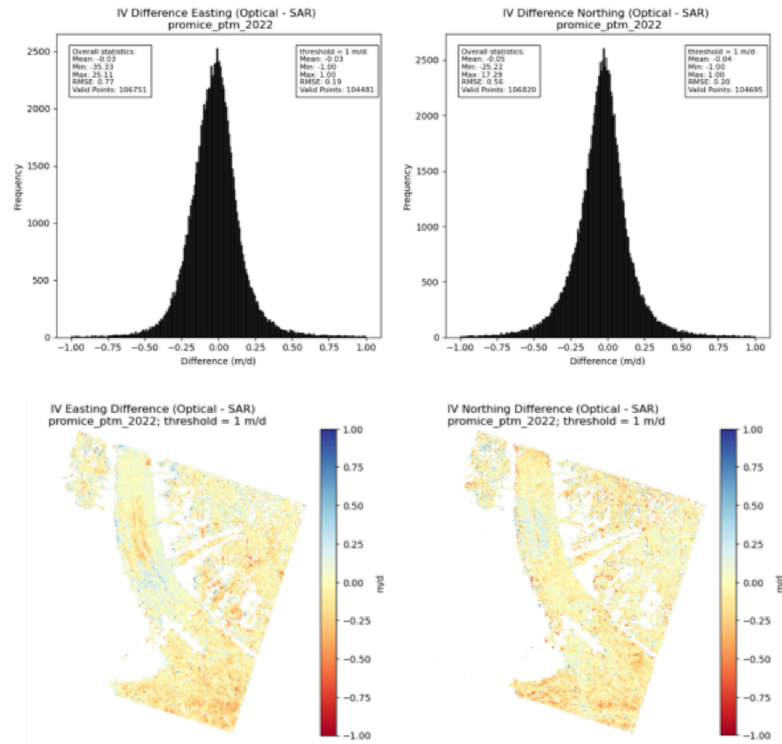
Figure 3-12 Petermann glacier easting and northing component intercomparison with PROMICE 2022 (see table 3-1 for exact time span of seasonal product).
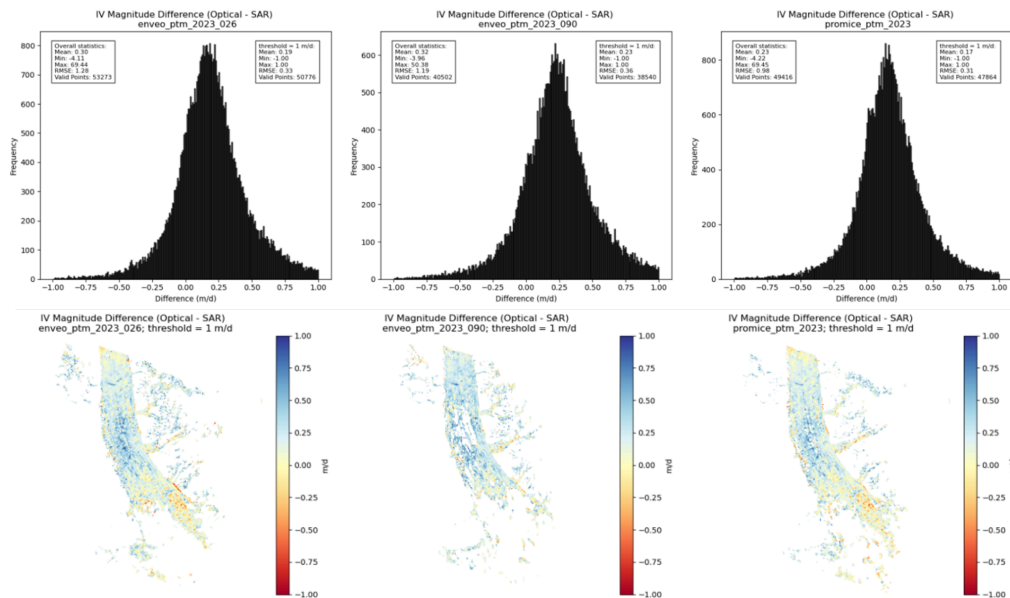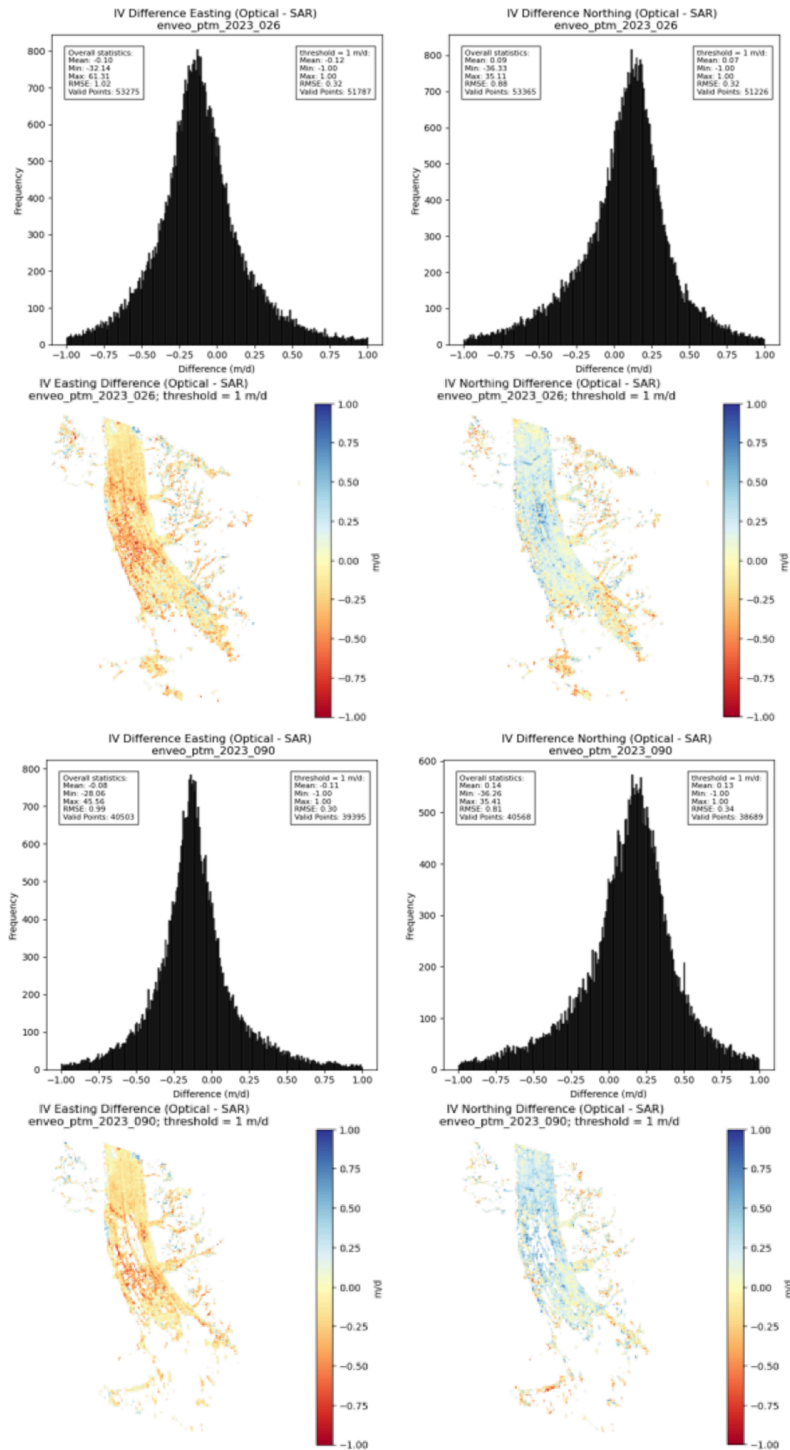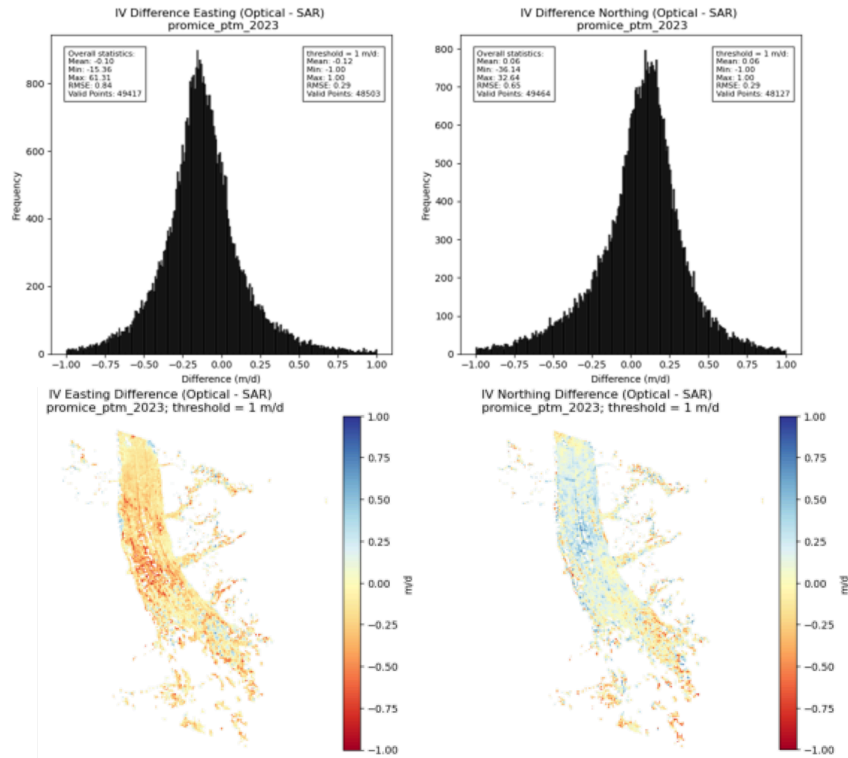

Figure 3-13 Petermann glacier magnitude intercomparison with ENVEO and PROMICE 2023 (see table 3-1 for exact time span of seasonal product).

Figure 3-14 Petermann glacier easting and northing component intercomparison with ENVEO 2023. Note that estimates for two different tracks were provided for Petermann, track 026 and 090 (see table 3-1 for exact time span of seasonal product).

Figure 3-15 Petermann glacier easting and northing component intercomparison with PROMICE 2023 (see table 3-1 for exact time span of seasonal product).

3.2.4 Recommendations for products improvement

The optical IV algorithm determines ice velocity (IV) by matching pixels between two images. Combined with the time difference between images, this shift calculation enables measurements of the ice velocity. Enhancements to feature tracking within this algorithm can significantly improve its accuracy. Specifically, refining the weighting of pixel pairs and improving velocity calculation methods can lead to more reliable ice velocity data.

One key area for improvement is the coregistration process, especially for large glaciers without visible coastlines. Currently, coregistration relies heavily on coastal features, which limits its effectiveness for inland glaciers. By developing a method that leverages neighboring tiles with coastlines for reference, the system can be adapted to analyze glacier areas further from the coast. This adjustment would enable the CCI IV algorithm to process data for a broader range of glacier locations, extending its applicability to regions previously unsupported.

Another important area for improvement relates to floating ice filtering. The current data products suffer from spurious signals coming from the ice melange and icebergs floating in front of the glaciers. Being characterized by sharp, traceable edges and a low velocity, the tracking algorithm does indeed calculate their velocity. In order to filter this spurious signal, a postprocessing step needs to be implemented. One of the possibilities recommended is to implement a postprocessing step based on pre-calculated Calving front locations (CFL). By filtering out what is located after the CFL, it would be possible to reduce the likelihood of erroneous measurements caused by floating ice.

4   Gravimetry Mass Balance (GMB)

This chapter gives a summary of the activities carried out to assess the quality of the GMB products.

There has been no direct validation of the GMB products because no independent data sets are available. Instead inter-comparisons have been carried out to assess the variability of these products arising from the use of different methods and data sets.

Previously, several inter-comparison exercises have been carried out. The results of these together with further investigations made on the specific CCI+ products are presented here.

4.1   (Inter-) comparison procedure

There are several (inter-)comparison strategies to follow. We focus on the mass change time series (and the trend in this) product and describe the following:

1. Comparison to other methods for regional and ice sheet mass balance. These are the Input-output method (or mass budget method) and volume change method.

2. Inter-comparison of the results from different methods for deriving mass changes from the same GRACE data

4.2   (Inter-) comparison procedure outcome

1.   A comparison of GRACE-derived mass changes to other methods for regional and ice sheet mass balance is a major task to undertake, and outside the scope of this document. Several of such studies have been published, and here we highlight a few. The IMBIE (ice-sheet mass balance inter-comparison exercise, Shepherd et al., 2012, 2018 and 2020; Otosaka et al., 2023) was an ambitious project including numerous methods and data sets.

The overall mass balance for ice sheets from different methods is seen in Fig 4-1. These are the Input-output method (or mass budget method) and volume change method.

It can be seen that the gravimetry method has mass balance results that agree with the two other methods within the error bars. Both methods, i.e. the point mass inversion and the tailored sensitivity kernel approach, which are used for generating the GIS CCI GMB products were also provided to the IMBIE study (Shepherd et al., 2018 and 2020; Otosaka et al., 2023).

2.   A detailed inter-comparison of the results from different methods for deriving mass changes applied on the same GRACE data was undertaken in the CCI GMB Round Robin Exercise (RRE). The procedure and the results are described in detail in Groh et al. (2019). Both methods used in the GIS CCI GMB production were included in the RRE and showed good agreement with other submissions.

Here, we present an inter-comparison of the CCI+ mass change time series products for the entire GIS (Fig 4-3) and individual ice drainage basins (Fig 4-4 and 4-5). Both methods agree very well inside their given uncertainties in seasonal signal as well as in trend. The agreement in trend improved in comparison to the PVIR of the previous phase which can be attributed to the implemented ellipsoidal correction in this phase. For individual ice drainage basins the trend slightly diverges (basin 5 and 6). This can be the result of differences in e.g. how the leakage is treated.
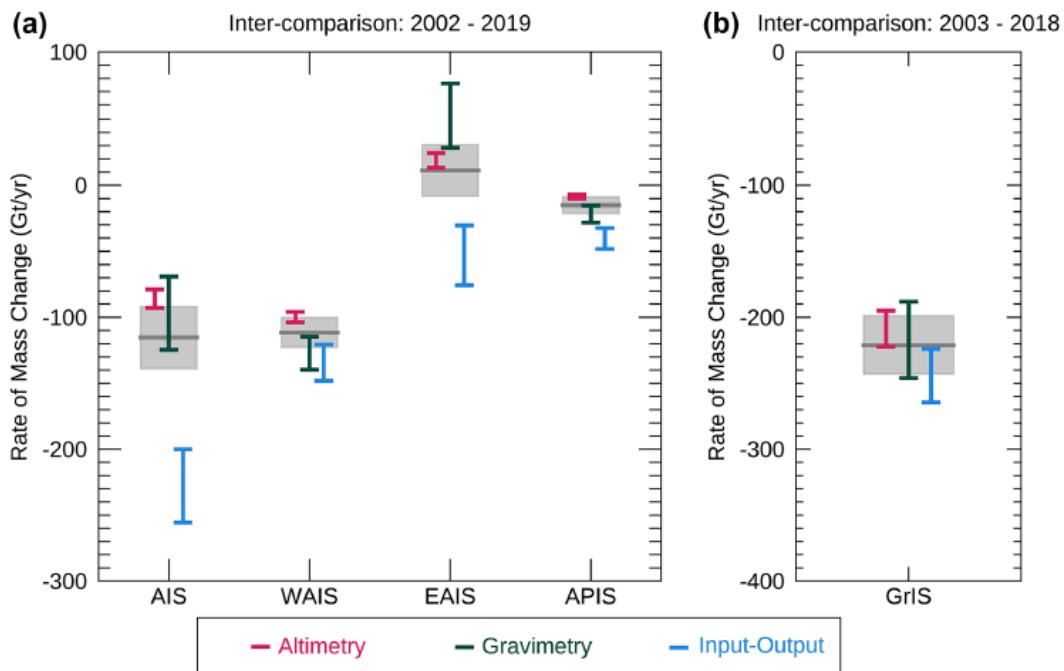
Figure 4-1: Mass balance of the ice sheets from different methods taken from Otosaka et al. 2023.
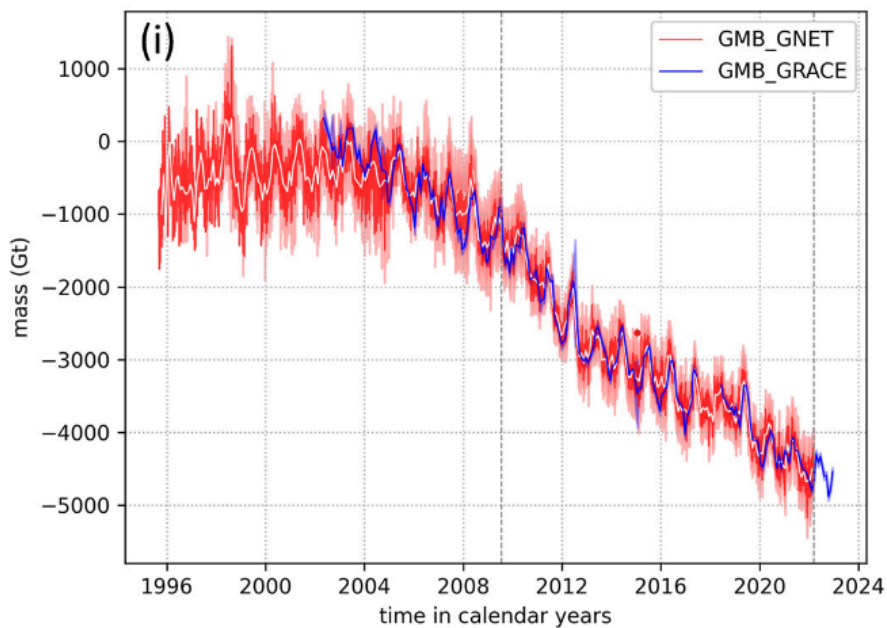

Figure 4-2: Another method presenting mass change time series of the entire GIS, from the GIS CCI GMB products derived by DTU (blue) and the daily derived GNET GMB product, taken from Barletta et al. 2024. The vertical dashed lines represent the working window (2009-2022) where more than 40 GNSS values per day were available and the GNET GMB are most reliable. Before 2008 only 30 GNSS were available, and only 10 before 2007. Only 4 GNSS stations were available before 2004.
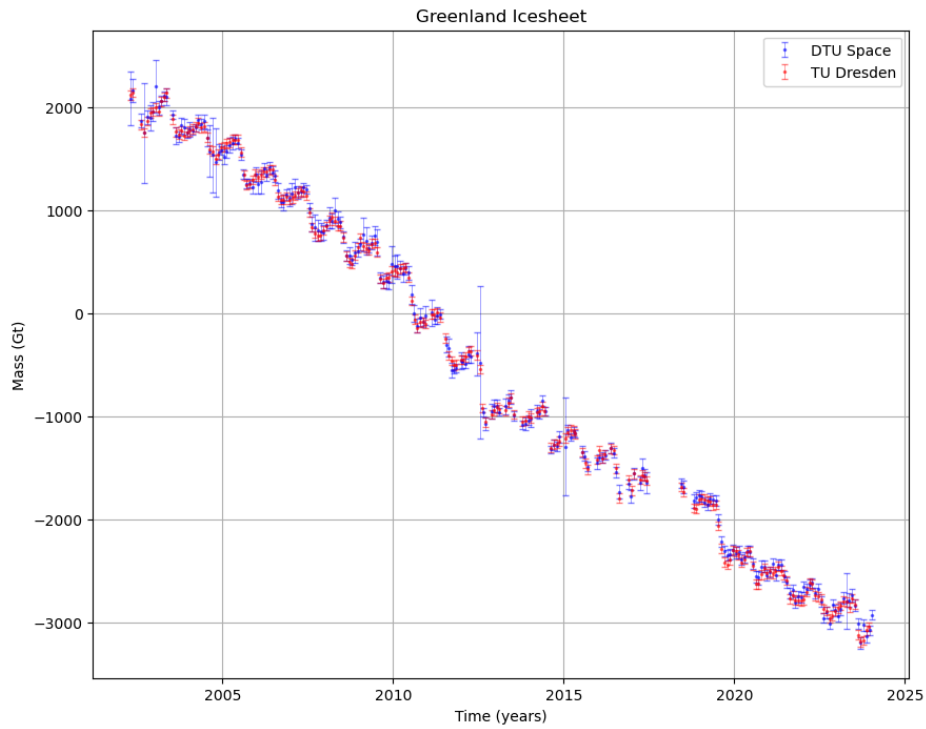
Figure 4-3: Mass change time series of the entire GIS, from the GIS CCI GMB products derived by DTU (blue) and TUDr (red).
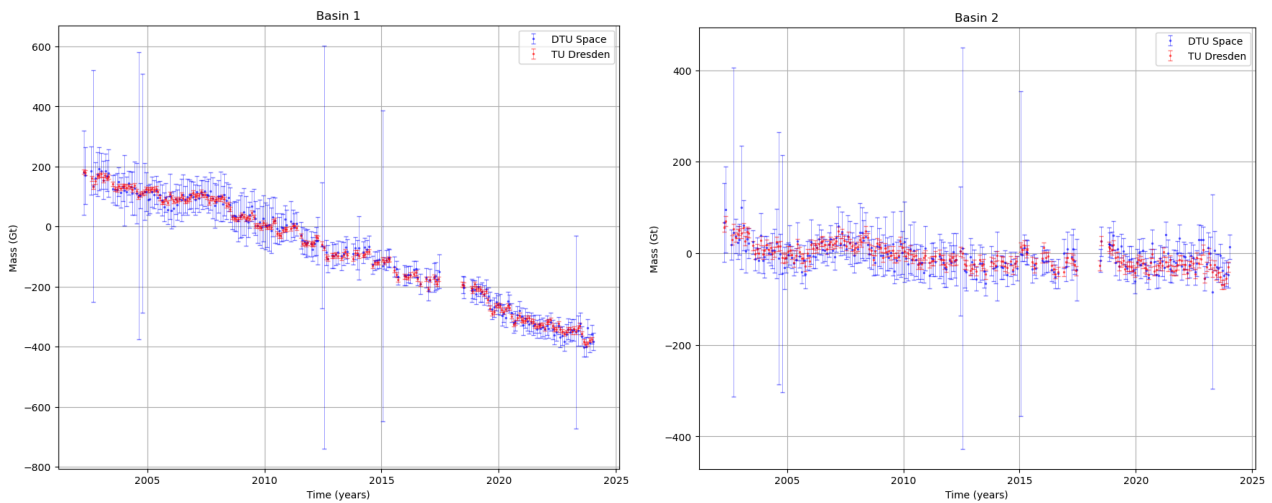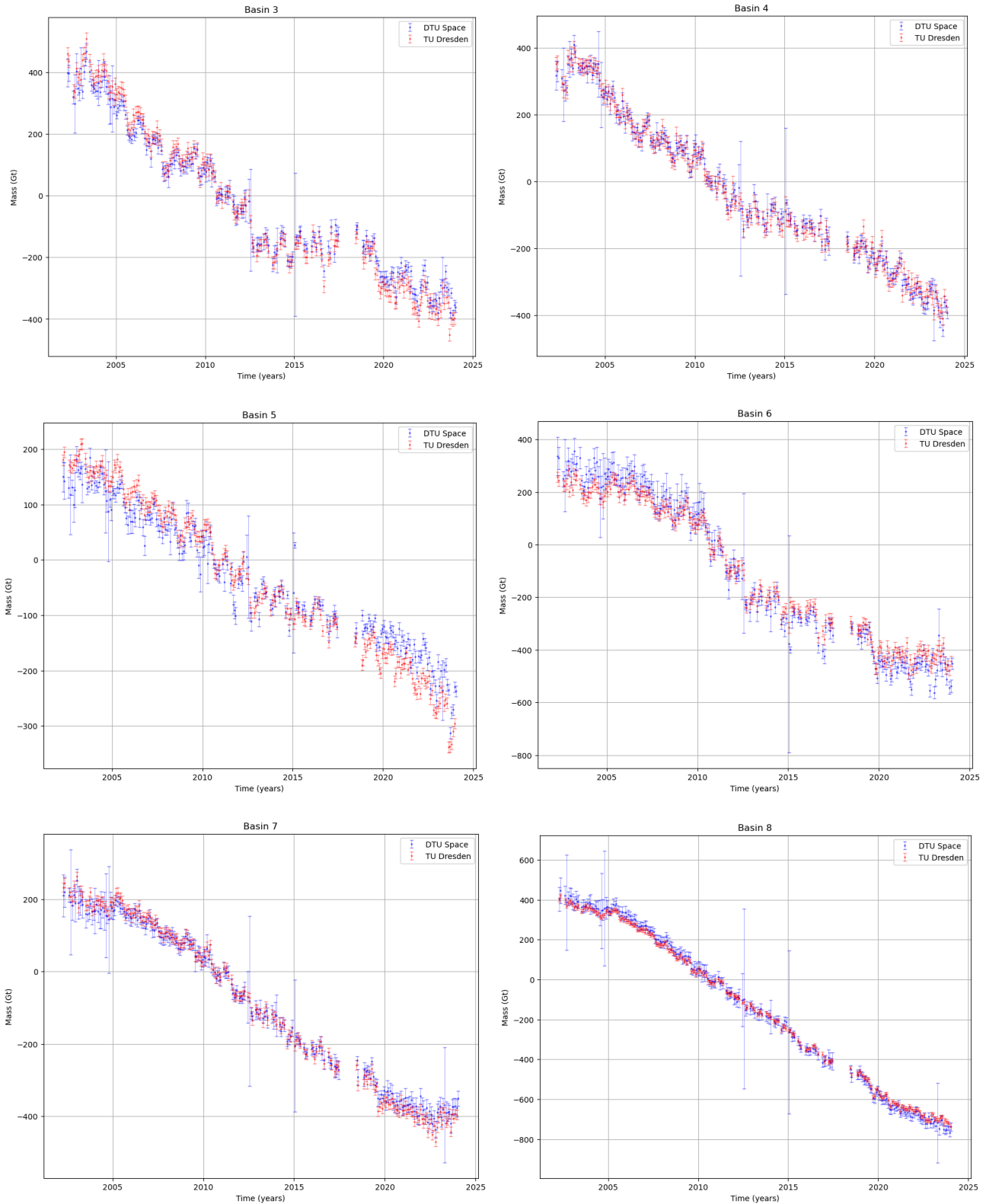
Figure 4-5 Mass change time series of basin 3 to 8 from the GIS CCI GMB products derived by DTU (blue) and TUDr (red).

4.3 Recommendations for products improvement

Improved correction models and methods

Better models for GIA, degree one, and ocean model correction will lead to future improvement in the products. Studies targeted on these corrections could lead to improvements in the products.

Improved uncertainty characterization.

Both GMB products (DTU and TUDr) employ different strategies for the uncertainty characterization. While both strategies agree well for the entire ice sheet over the whole timespan (Fig. 4-2), they disagree for individual drainage basins and single months. The DTU uncertainty characterization utilises the formal uncertainties of the level-2 data and propagates them to the GMB product. The TUDr uncertainty characterisation is based on separating the signal content and noise of the resulting time series. An improved uncertainty characterization would take into account both approaches and lead to a better agreement and more realistic uncertainties.

Until now only the basin products include the uncertainty characterization. Further developments to include uncertainties for the gridded product would improve the gridded product.

Partitioned Gravimetric Mass Balance.

The current GMB product represents the sum of two effects: (a) Effects of changing ice-flow dynamics and (b) Effects of variations in surface mass balance (SMB). Both effects differ in their timescales, forcing, and impact on the climate system and environment. Partitioning the GMB into mass balance due to SMB fluctuations and dynamic and long-term mass balance would give a new ECV product which builds directly on the GMB product. Such ECV would benefit applications like e.g., sea-level projects and their current uncertainties which are mainly related to the long-term evolution of the ice-flow dynamics imbalance. First demonstrations of the partitioning have been carried out for the Antarctic ice sheet using modelled SMB.

Integrated CryoSat-2, GRACE and Sentinel-1 data.

One issue with the GRACE-only products is the low spatial resolution and therefore one recommendation is to produce products with increased resolution. This could be done from integrated CryoSat, GRACE and Sentinel-1 data, combined with firn compaction and snow surface density meteorological models.

The mass changes of the Greenland ice sheet are measured directly with GRACE, but only with limited spatial resolution, and relatively large errors associated with leakage from oceans, land, and other ice caps. Combining CryoSat and GRACE data, supplemented with a firn density and compaction model, an integrated mass solution can be obtained with high spatial resolution. Noting that rapid temporal changes of the ice sheet is primarily driven by rapid changes in velocities of outlet glaciers, which can now be monitored at weekly resolution by Sentinel-1, the combination of all three EO data sources – GRACE, CryoSat altimetry and Sentinel-1 ice velocities – into a unified mass product, will give a new enhanced experimental ECV product, superior to the existing CCI SEC, IV and GMB products. This enhanced product will represent an operational product following the IMBIE principles and can easily be extended to Antarctica as well at a later stage. The first concept demonstration results of such activities, for both Greenland and Antarctica, has been published in Forsberg et al. 2017. A similar approach has been realized by Kappelsberger et al., 2021 for Greenland.

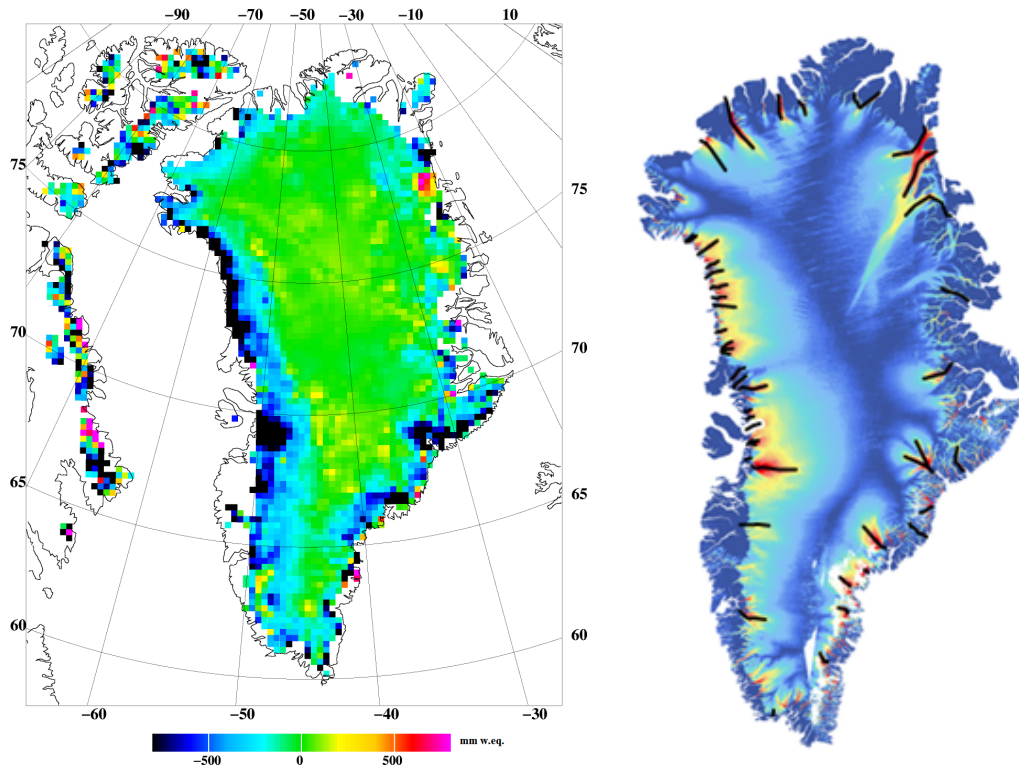|	Greenland_Ice_Sheet_cci+ Product Validation and Intercomparison Report (PVIR) for CCI+ Phase 2	Reference: DTU-ESA-GISCCI+-PVIR-002
greenland ice sheet cci		Version : 1.0 page
		Date : 16 December 2024 39/56

Fig. 4-6. GRACE/CryoSat mass balance grid of Greenland (left, low-resolution demonstration product) will be combined with Sentinel 1-A (and later –B) ice velocities from the Greenland ice sheet (right) in the proposed CCN/CCI+ action. Current S-1 acquisition scheme allow sub-monthly estimation of essentially all Greenland outlet glaciers.

5 Mass Flow Rate and Ice Discharge (MFID)

The MFID product is validated against all known estimates of ice discharge that are available at the spatial (sector, Zwally *et al.* (2012)) and at least annual resolution. This includes three completely independent plus one different dataset of ice discharge. The independent estimates come from external parties while the "different" dataset is produced PROMICE (Mankoff, Solgaard and Larsen, 2020), using a similar algorithm as MFID, but using other data sources and tuned differently. That is, the PROMICE validation data set is generated with gates in different locations and using a different cutoff velocity than this CCI+ work. Due to algorithm changes in Phase 2, we also validate against the MFID from Phase 1.

5.1 Sources and selection of independent validation data

Independent data comes from King *et al.* (2020), Mouginot *et al.* (2019), ENVEO (2024), and PROMICE (Mankoff, Solgaard and Larsen, 2020). King *et al.* (2020) provides discharge estimates at monthly temporal and glacier spatial resolution. Mouginot *et al.* (2019) provides discharge estimates at *annual* temporal and sector spatial resolution. The PROMICE estimate provides discharge at ~12-day temporal and glacier spatial resolution. Although Mouginot *et al.* (2019) is only an annual resolution, this should not significantly impact results which according to King *et al.* (2018) only vary by ~6 % seasonally.

5.2 Validation procedure

We downsample the PROMICE and King *et al.* (2020) data to monthly temporal and basin spatial resolution, by averaging in time and summing in space, and then compare to this product that already exists at that resolution. The Mouginot *et al.* (2019) product remains at annual temporal resolution. We then graphically display this product (CCI+), with all of the other products, in individual plots per sector (Zwally *et al.* (2012)) and one Greenland wide plot. We then visually compare the lines in the graphics. The comparison with the ENVEO estimate is only done on a Greenland wide scale.

Additionally we also compare to the CCI+ phase one estimate (black dashed line), where the main update is the method used to estimate the ice thickness at the flux gates. The updated method is outlined in the ATBD.

5.3 Validation procedure outcome

All the estimates overlap within the uncertainty limits. Some sectors do have outliers, however the CCI+ product is never the outlier and always falls within the uncertainty estimates of the majority of the other comparable discharge products.

The CCI+ Phase 1 and Phase 2 products match in most sectors. Only minor differences were detected in sectors 3.2, 4.1, 4.3 and 5.0. These differences can generally be attributed to significant updates in the bed topography in the bed machine dataset used to provide the ice thickness estimates in these sectors. Additionally, sector 4.1 is dominated by the Helheim catchment and is highly sensitive to the flux gate location which can be an additional factor attributing to the discrepancy seen between the CCI+ estimates and the PROMICE estimate.

In the final complete total Greenland Ice Sheet wide intercomparison between all estimates shows very good agreement, despite difference in methods and input datasets. The CCI+ phase 1 and Phase 2 estimates lay very centralised within the other estimates and well within the uncertainty of all other estimates.

5.4 Recommendations for products improvement

The surface elevation changes are currently based on 5-year averages until 2019 and 1-year averages in the following years, and should be updated to match the monthly resolution of the IV in the next version, now that the monthly SEC is available. The positioning of the flux gate has an impact on the MFID estimates as the SMB below flux gate is currently not accounted for. It is recommended to apply the monthly SEC data (dSEC) to the areas downstream of the flux gates to account for the mass loss from melt to reduce the uncertainty in the MFID estimates. Additionally this will reduce the bias in the flux gate location, as some flux gates are placed higher upstream than others and so the uncertainty in each location can vary in the current product.
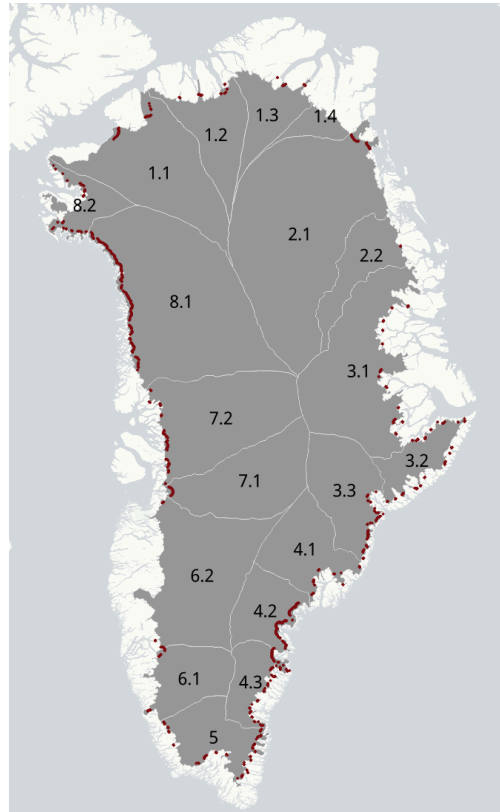
Figure 5-1a: Overview of all the Zwally et al. (2012) basins used in the intercomparison. The flux gates of the marine terminating outlets are annotated in red.
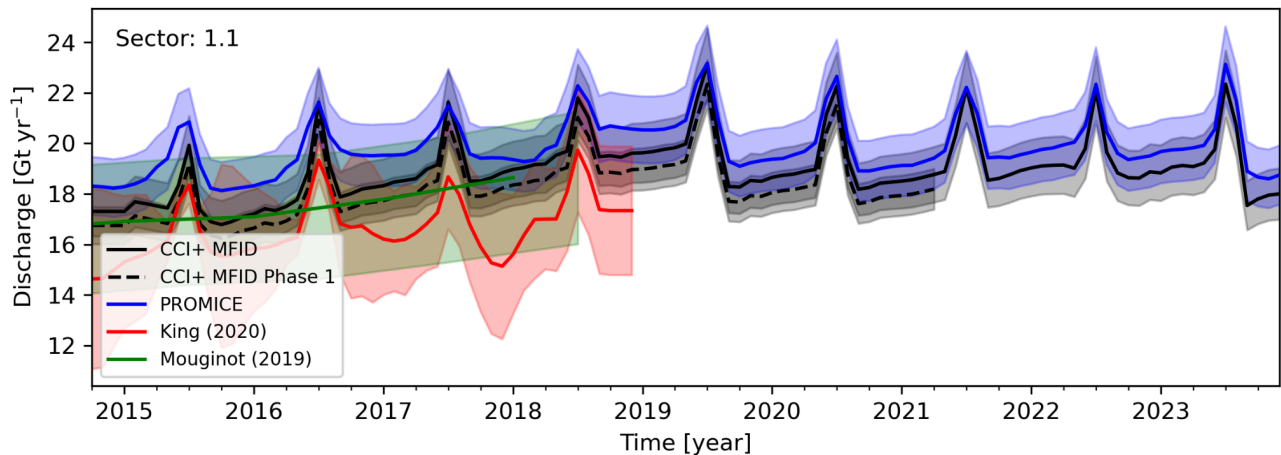

Figure 5-1b: Comparison between this product (CCI+ MFD; black), CCI + Phase one (black dashed), PROMICE (blue), King et al. (2020) (red), and Mouginot et al. (2019) (green). Uncertainty estimates come from the respective published products or described in the ATBD and uncertainty documentation for the CCI+ product. Sector label from Zwally et al. (2012) is printed in top-left corner of graphic.
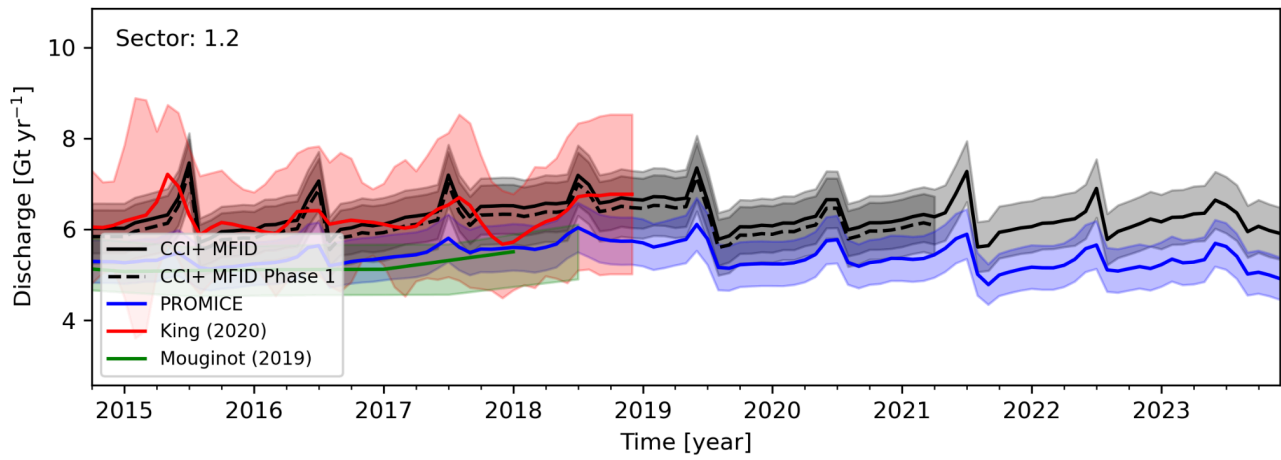
Figure 5-2: Same as Figure 5-1 caption.
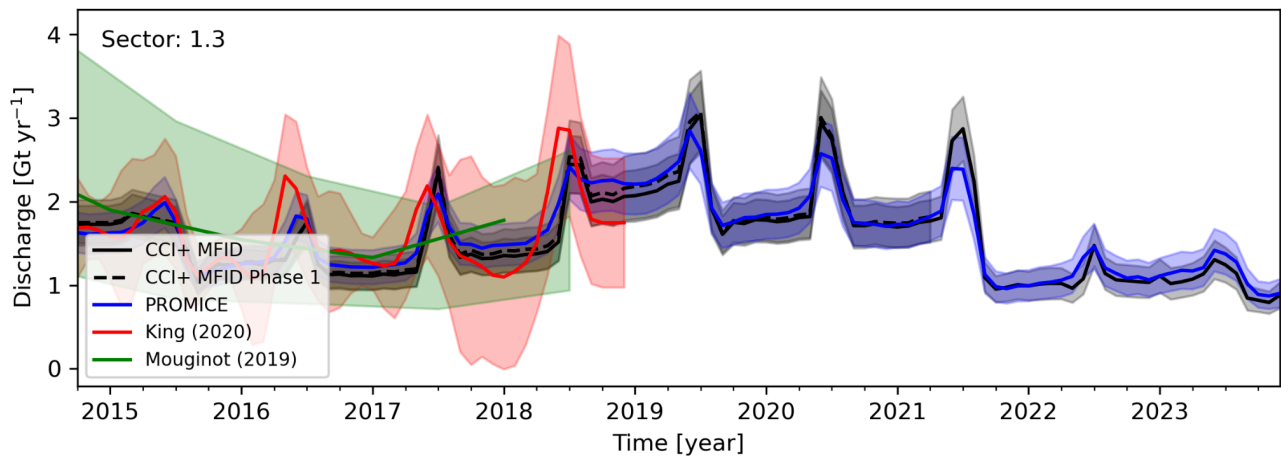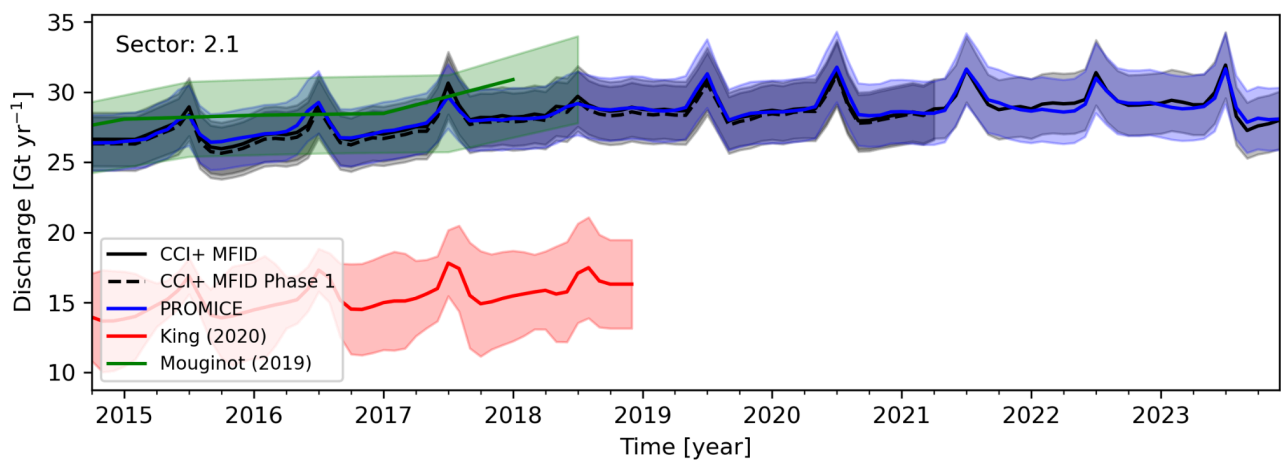

Figure 5-3: Same as Figure 5-1 caption.
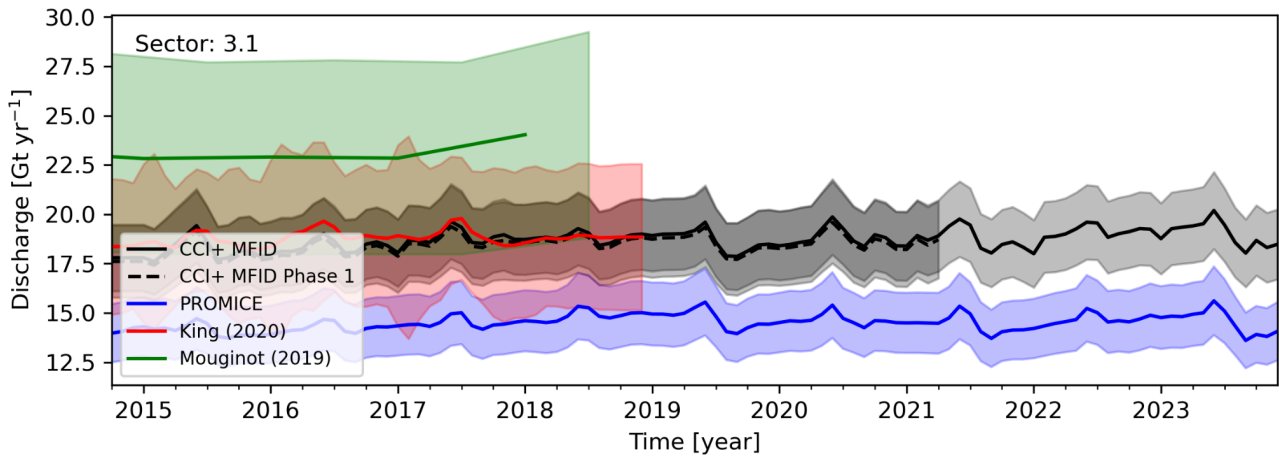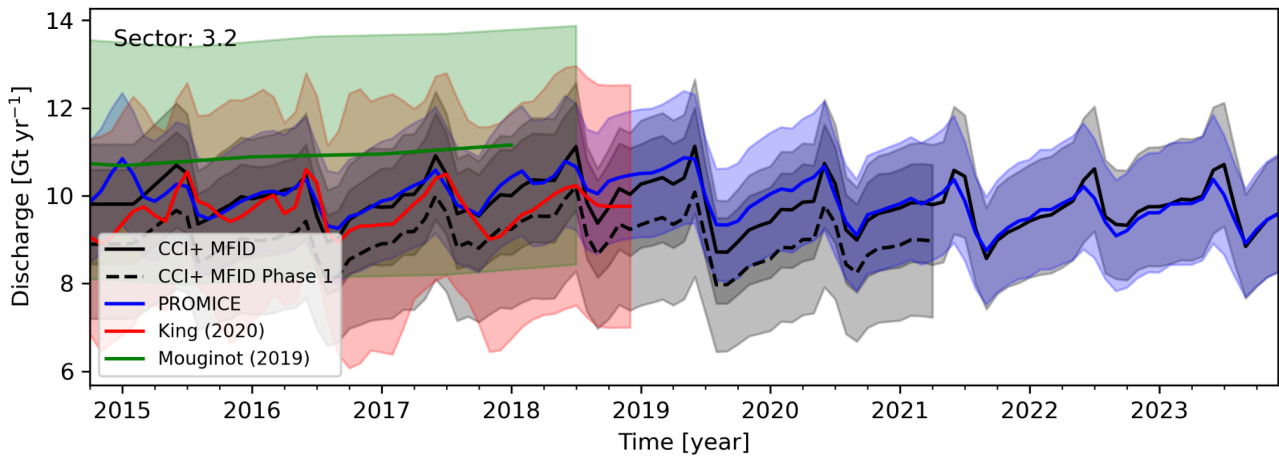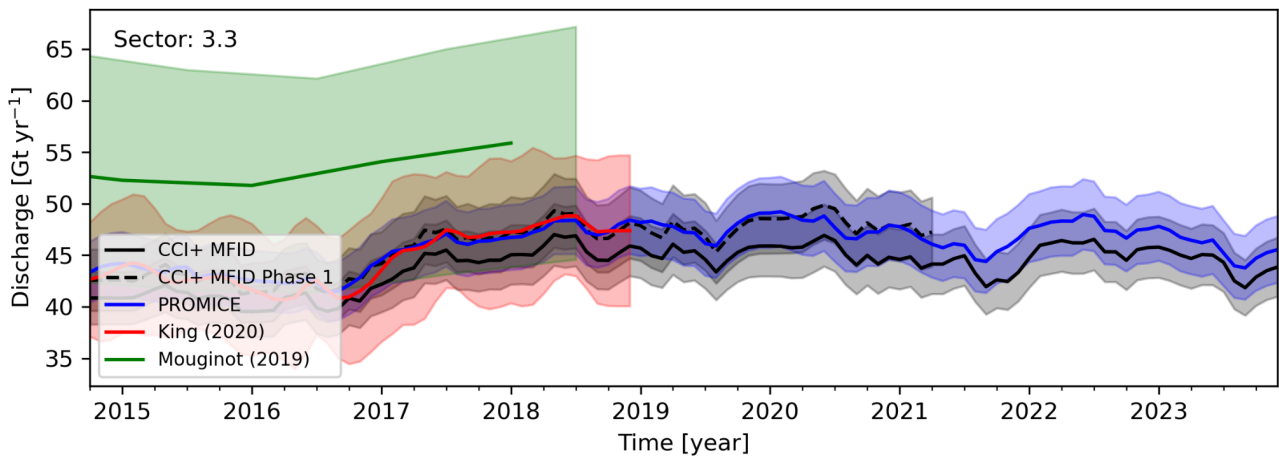

Figure 5-4: Same as Figure 5-1 caption.

Figure 5-5: Same as Figure 5-1 caption.

Figure 5-6: Same as Figure 5-1 caption.

Figure 5-7: Same as Figure 5-1 caption.

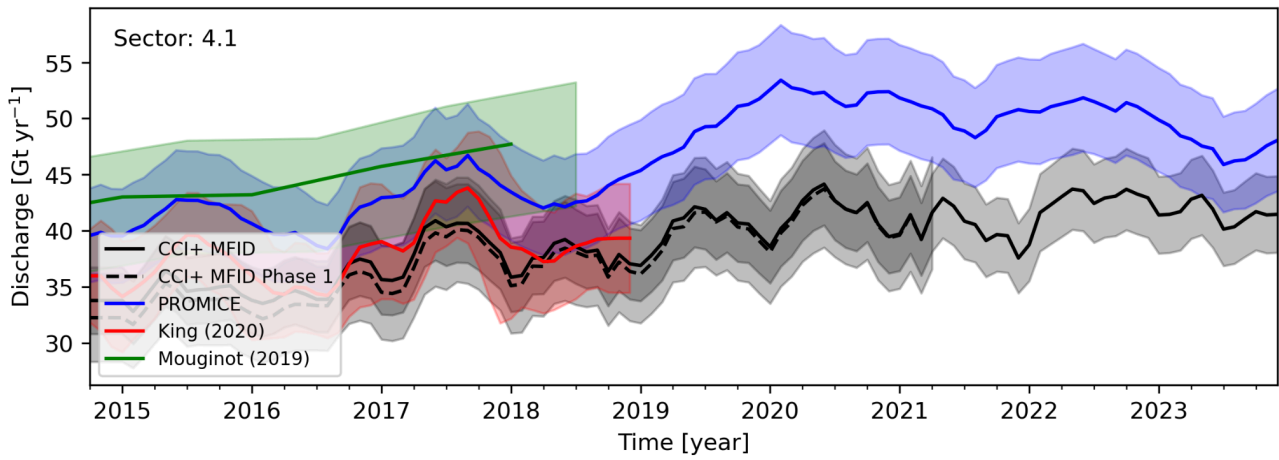|	Greenland_Ice_Sheet_cci+ Product Validation and Intercomparison Report (PVIR) for CCI+ Phase 2	Reference: DTU-ESA-GISCCI+-PVIR-002
greenland ice sheet cci		Version : 1.0 page
		Date : 16 December 2024 44/56

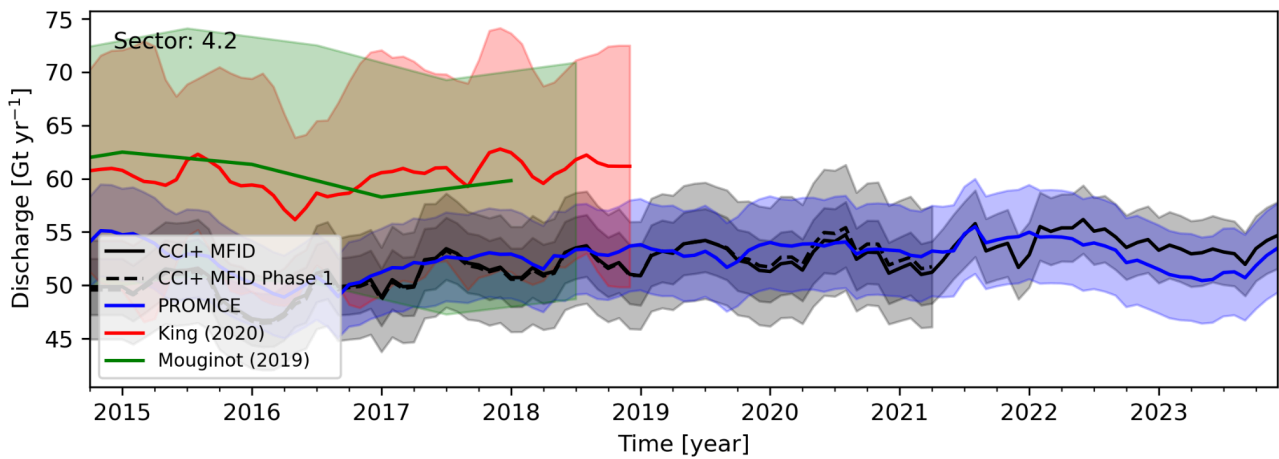*Figure 5-8: Same as Figure 5-1 caption.*

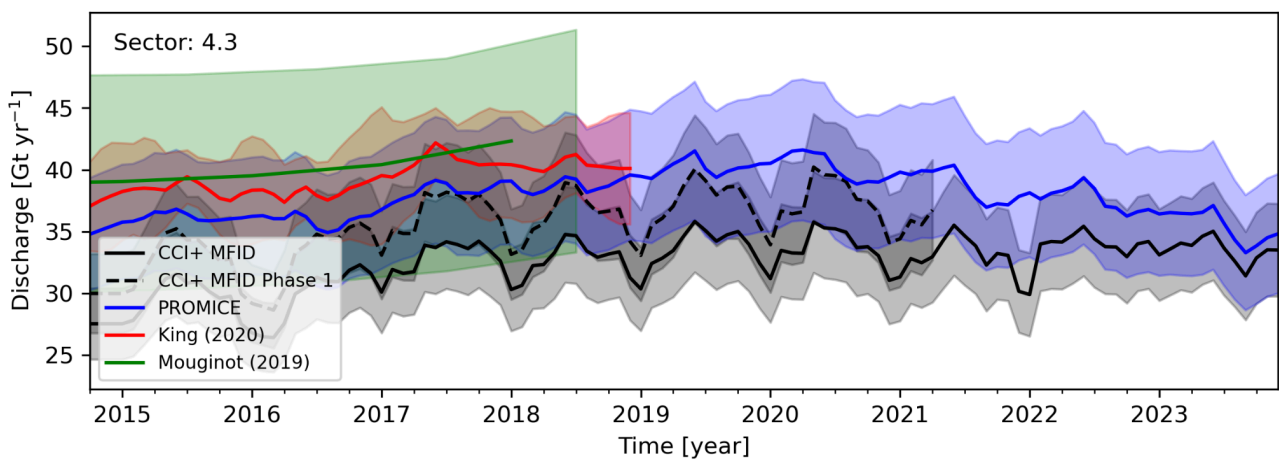*Figure 5-9: Same as Figure 5-1 caption.*

Figure 5-10: Same as Figure 5-1 caption.

Figure 5-11: Same as Figure 5-1 caption.

Figure 5-12: Same as Figure 5-1 caption.

Figure 5-13: Same as Figure 5-1 caption.

Figure 5-14: Same as Figure 5-1 caption.

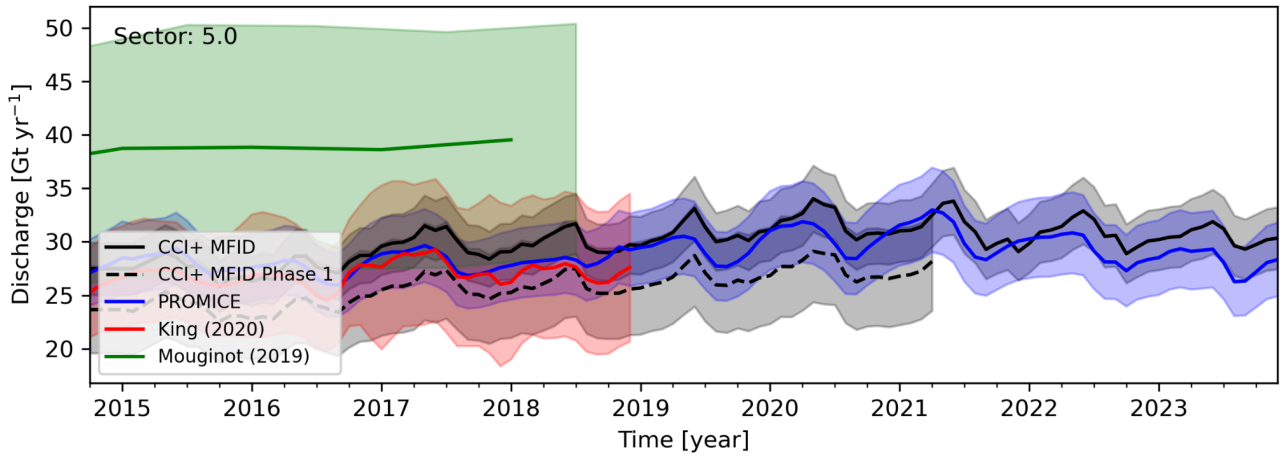**Figure 5-15: Same as Figure 5-1 caption.**
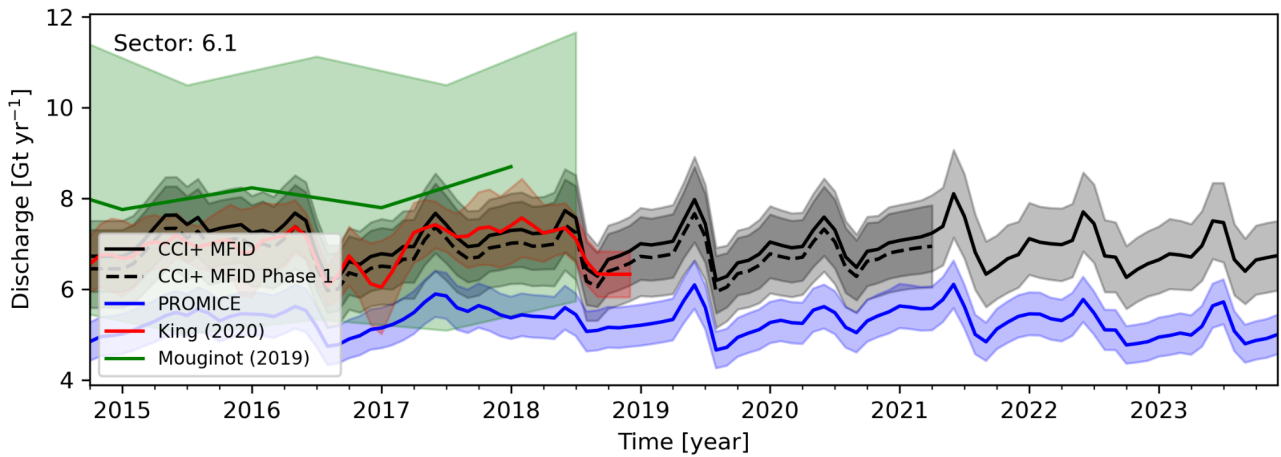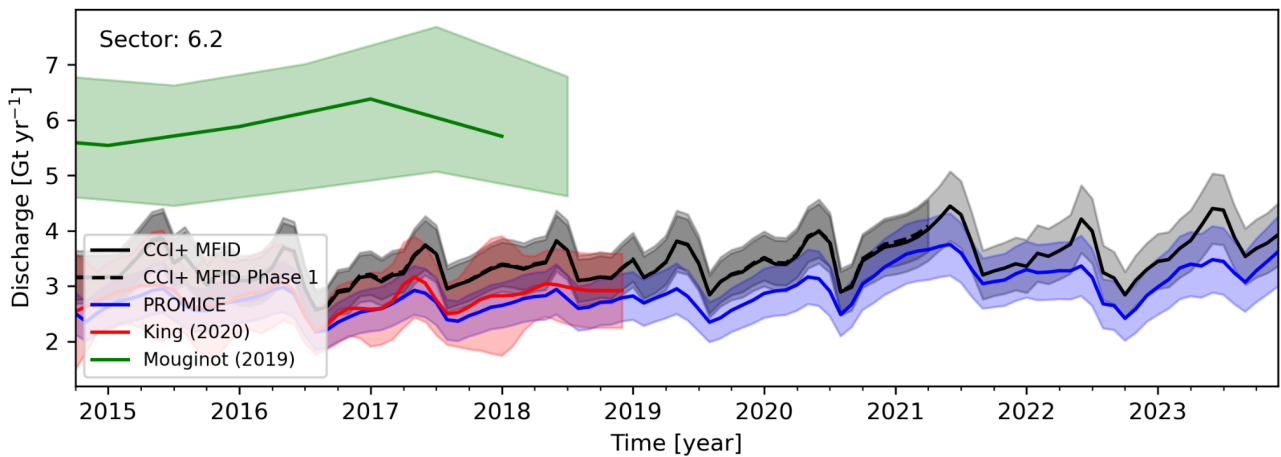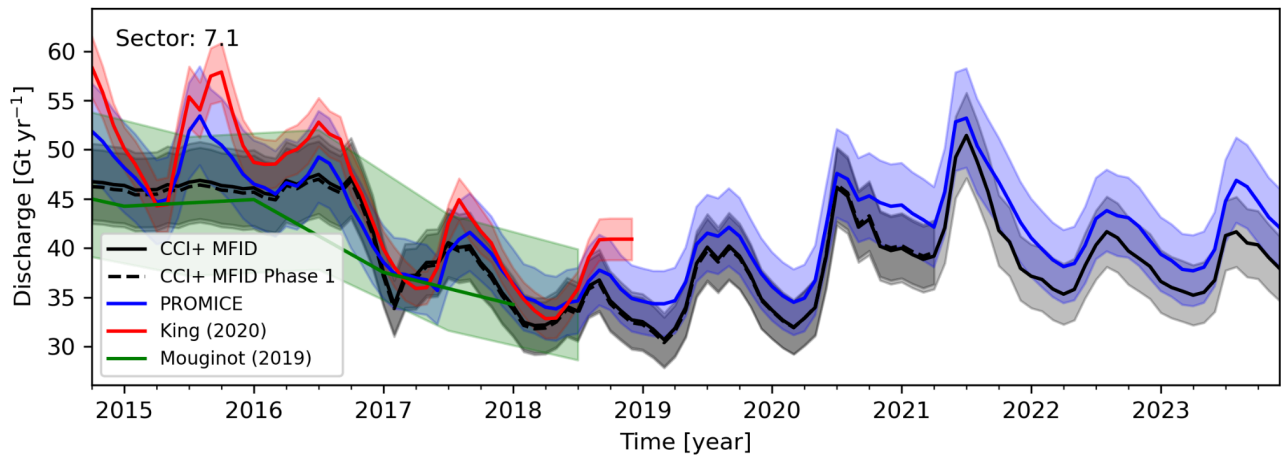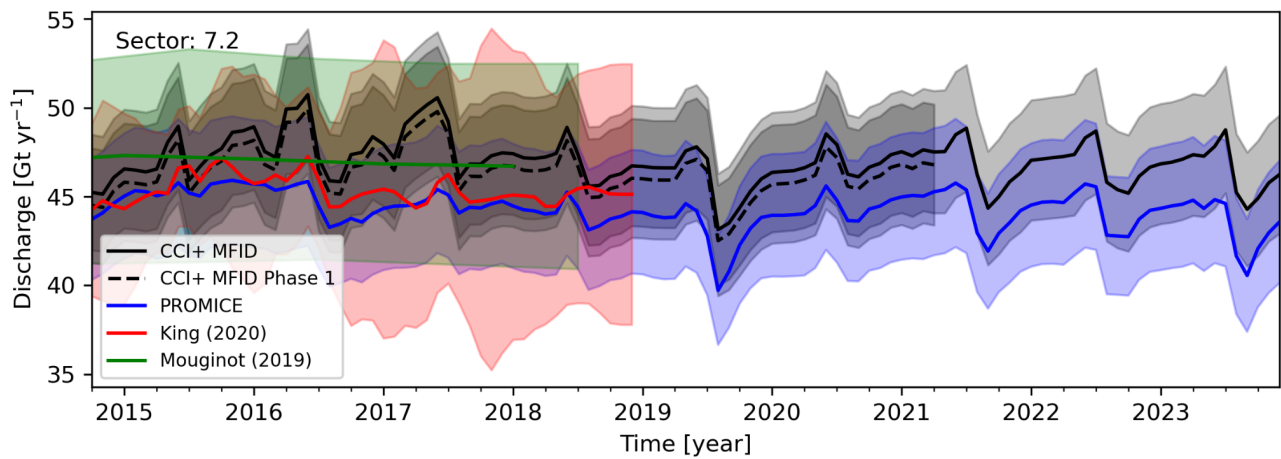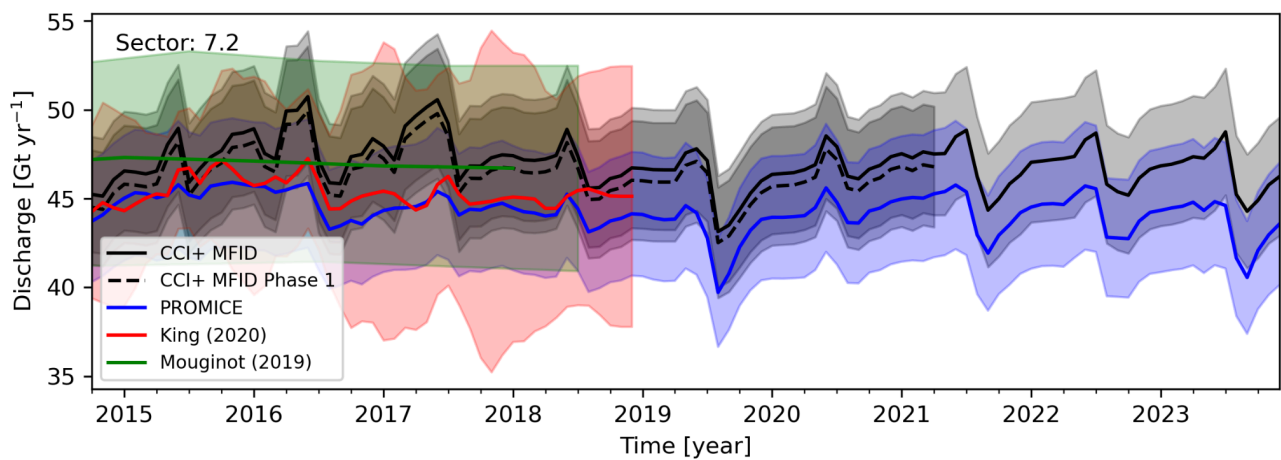
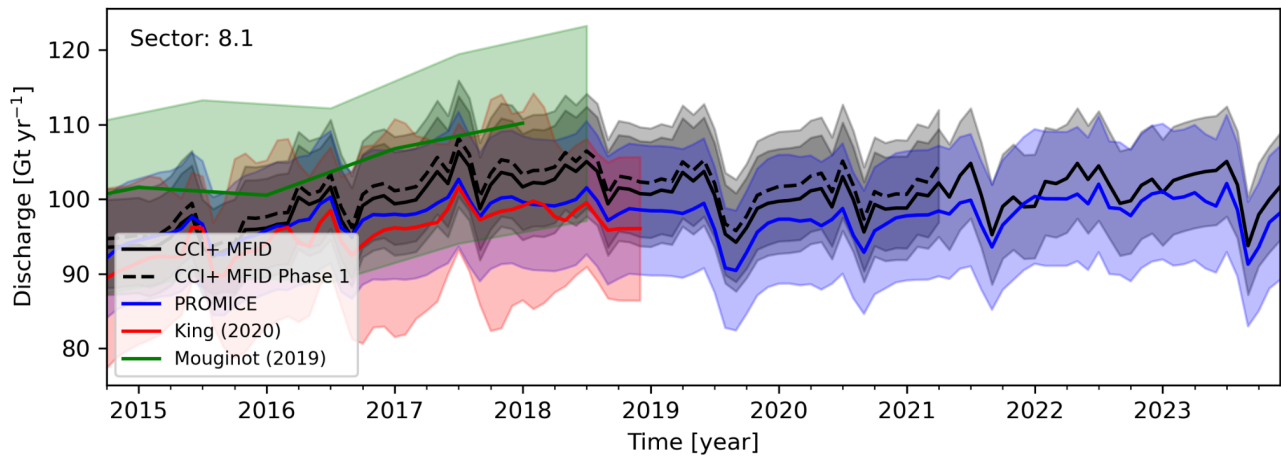

Figure 5-16: Same as Figure 5-1 caption.
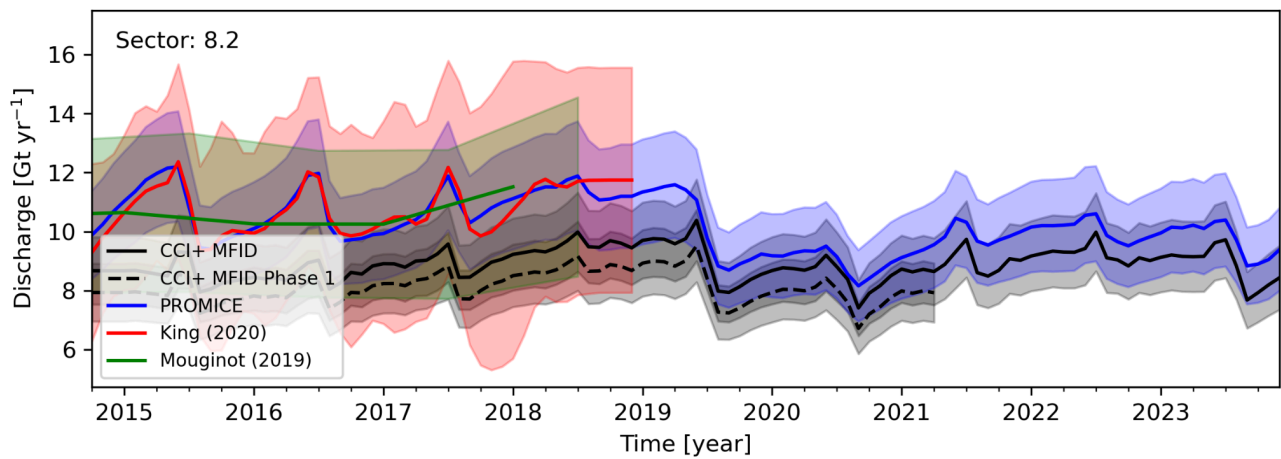
Figure 5-17: Same as Figure 5-1 caption.
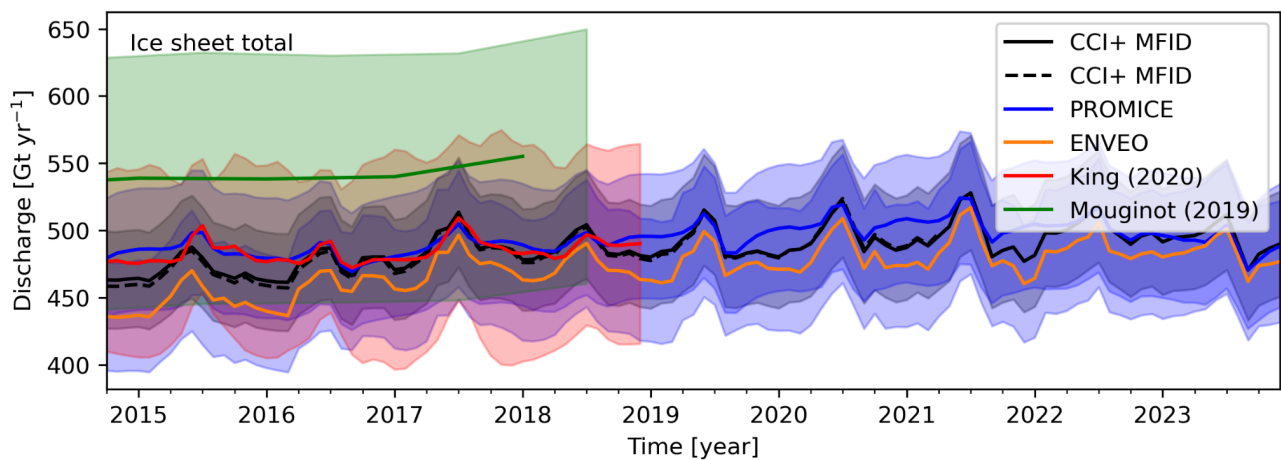

Figure 5-18: Same as Figure 5-1 caption.

Figure 5-19: Total Greenland wide intercomparison including the addition of the ENVEO estimate (orange).

6   Supraglacial Lakes

Supraglacial lakes (SGLs) have been identified and modelled across the Nioghalvfjerdsbrae (79N) and Sermeq Kujalleq (SK, also known as Jakobshavn Isbræ) catchments for the melt season 2019. Earlier SGL identification over SK have resulted in over 6000 (±15%) lake features identified over the melt season, with an average lake area of 0.4 km^2 (±22%). With the maximum number of lakes evident during the peak melt season.

In previous phases we have included a version of an SGL product to the Greenland Ice Sheet CCI+ project (GIS CCI+). The argument for including this as a product is the importance as an R&D product for understanding glacier dynamics, particularly w.r.t. lake extent and drainage (e.g. Das et al., 2008; Andrews et al., 2018).

Being able to produce validated depth estimates would further aid this effort of understanding. For this reason, validation of a dual lake extent & lake depth product would greatly increase the value of the produced product. Furthermore, the increased revisit-rate from using S2-data, with similar metrics as one can get for IS2-based depth estimates, could result in a significantly better time-wise sampling rate.

Previous studies using remote sensing have been conducted on the GIS, derived from multiple different instruments that include MODIS, Landsat, Sentinel-2, etc. (Hoffman et al., 2011; Liang et al. 2012; Williamson et al., 2017; Rowley et al., 2019). Validation still relies on intercomparison of temporally colocated samples, if available, due to the lack of an idealised dataset of SGLs (e.g. Rowley et al., 2019, and Liang et al., 2012).

6.1   Sources and selection of independent validation data

Landsat-8 imagery is used for the sensor inter-comparison, adopting the detection method used for the SGL product to derive supraglacial water bodies from coinciding Landsat-8 scenes. Scenes were selected based on three key criteria: 1) cloud cover (less than 60%); 2) spatial coverage (across the entire monitoring area used for the SGL product); and 3) corresponding with Sentinel-2 image acquisitions (less than 24 hours). The selected scenes are outlined in Table 6-1.

Table 6-1: Selected Landsat-8 scenes as validation data for 79N.

Scene IDs	Acquisition date	Cloud cover	Path Row
LC08_L1TP_007003_20190820_20200827_02_T1	20.08.2019 14:45:13	2.87 %	007 003
LC08_L1TP_007004_20190820_20200829_02_T1	20.08.2019 14:45:37	13.07 %	007 004

Table 6-2: Selected Landsat-8 scenes as validation data for SK.

Scene IDs	Acquisition date	Cloud cover	Path Row
LC08_L1TP_009011_20190818_20200827_02_T1	18/08/2019 15:00:45	2.78	009 011

6.2   Validation procedure

Landsat-8 scenes outlined in table 6-1 were used for the comparison of the proposed ML model, where a manual selection of lakes was chosen for comparison. These were selected to be representative of the various types of lakes that occur on the glacier. A total of 15 lakes were validated on the 79N glacier, Figure 6.1, and a further 8 were validated over the SK glacier, (Figure 6.2) for a total of 23 lakes.

The lakes were compared on their depth estimates and extents, though there were here some misalignment between the coregistration, causing a shift that made direct comparisons difficult. Landsat-8 data was preprocessed following the outlined procedure in https://www.usgs.gov/landsat-missions/using-usgs-landsat-level-1-data-product.

During this procedure selected bands were blue, green, red, and panchromatic, i.e. band 2, 3, 4, and 8. Pansharpening was applied to the first three bands for further processing. Lakes were manually delineated, and depths were estimated using the physically-based radiative transfer model (Philpot, 1989; Pope et al, 2016; Sneed and Hamilton, 2007). Lake depth was calculated using red and panchromatic band, and subsequently averaged.

6.3   Validation procedure outcome

Compared to earlier products that focus on single-feature prediction, the lake extents seen in the validation have some systemic errors to them. These errors are of a type where conditional post-processing can be performed to close holes in the lake extent predictions, something that was not performed ahead of validation. Similarly there are methods that were not included in the training of the chosen models that would be more reliable w.r.t closing the lake predictions.

When analysing the predicted depths, there is a clear bias shown in predicting the glaciers as having a depth overall (Figure 6.5) . This was to be expected with sparse data isolated only to a few crossings of lakes, and a model trained using regression. A slightly more troubling issue is the occurrence of mid-lake bulges towards a mean depth, which seems to be an issue pertaining to the receptive field / distance from the lake-edges. This is most clearly seen in the cross-sections of lakes, and the clearest example is seen in (Figure 6.6), showing the phenomenon on lake 3 in the 79N glacier scene.

Furthermore there is a tendency to underestimate depths of lakes, seen in Figure 6.4 even when compared to red-band reflectance based estimates. This was to some extent expected due to the depth-limitations of the training data. Some of these issues are related to issues seen in other ML-based depth-estimates of lakes, and we believe that this is another issue that could be addressed by more data, specifically depth-data.

An overall outcome is the clear indication that, while this form of modelling may seem promising, the current coverage seems insufficient to claim a comprehensive product can be delivered based on the models at this stage.
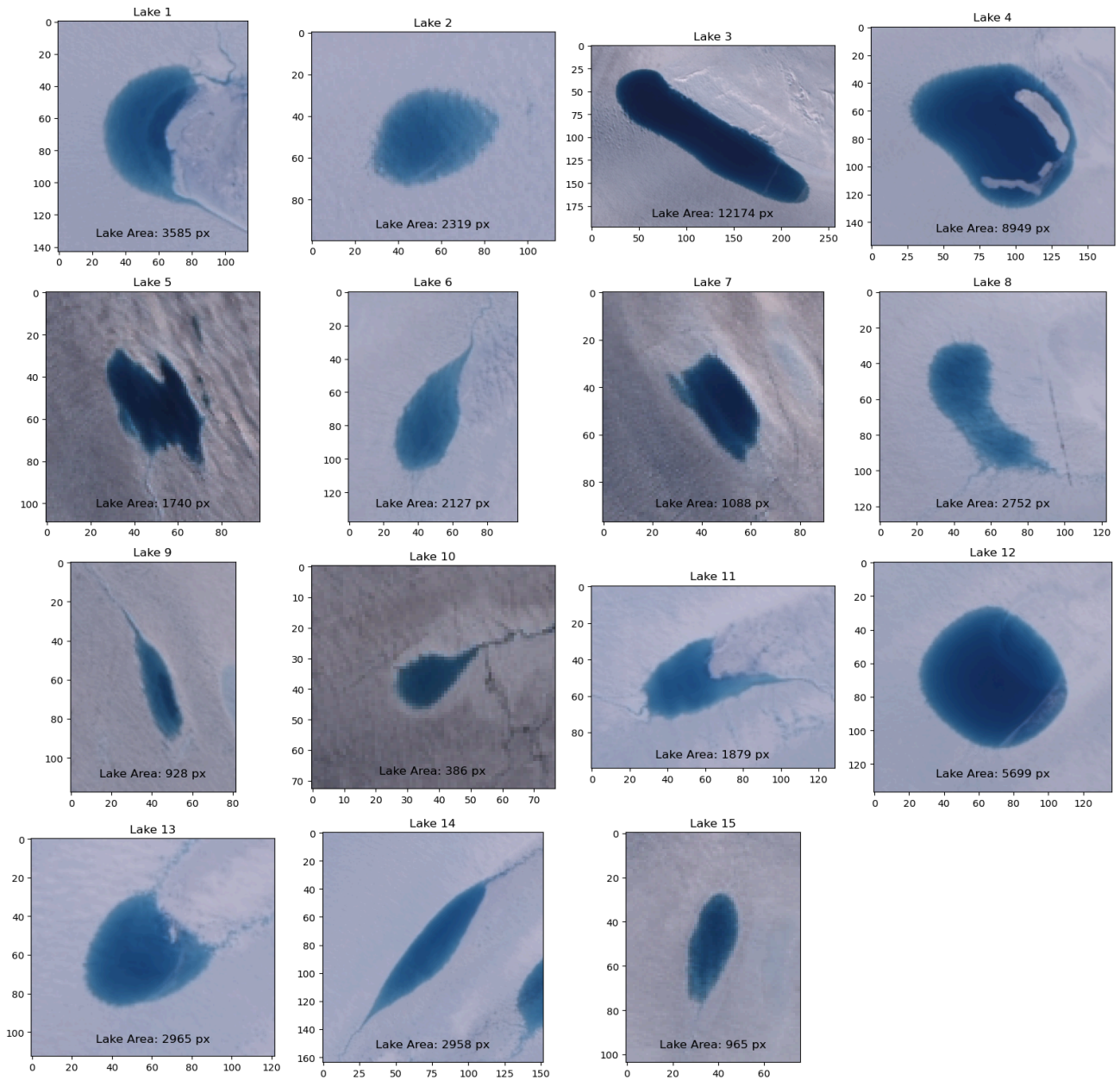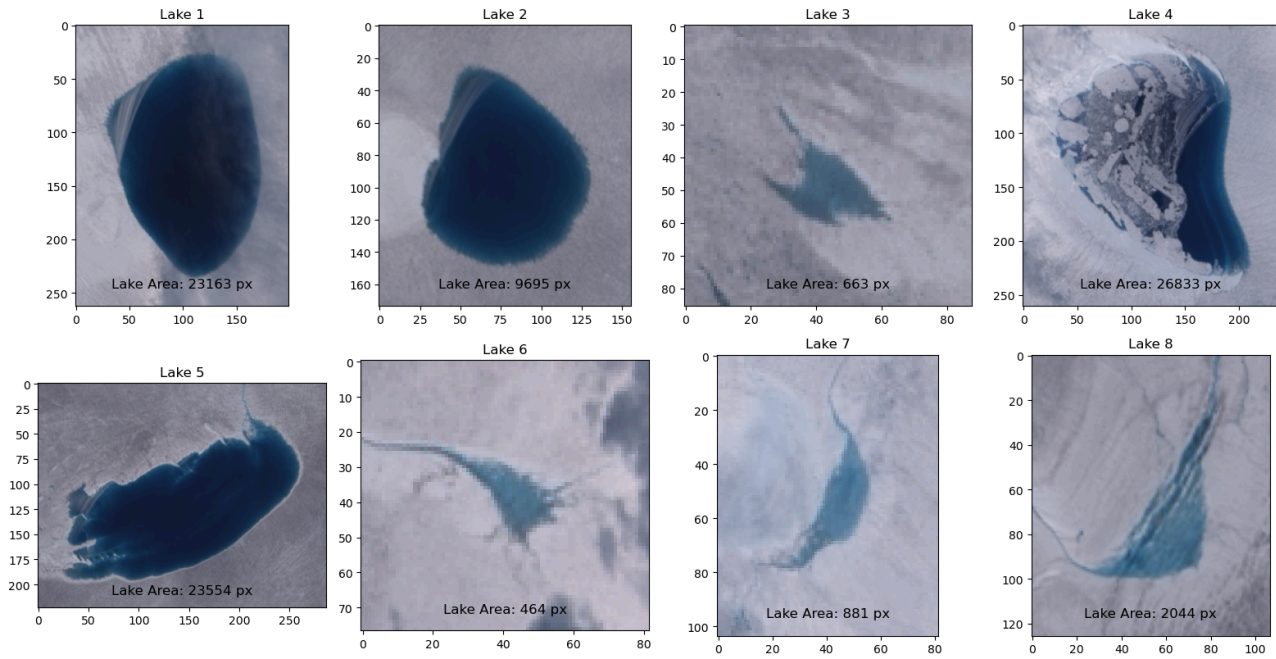
Figure 6.1: Selected lakes on 79N

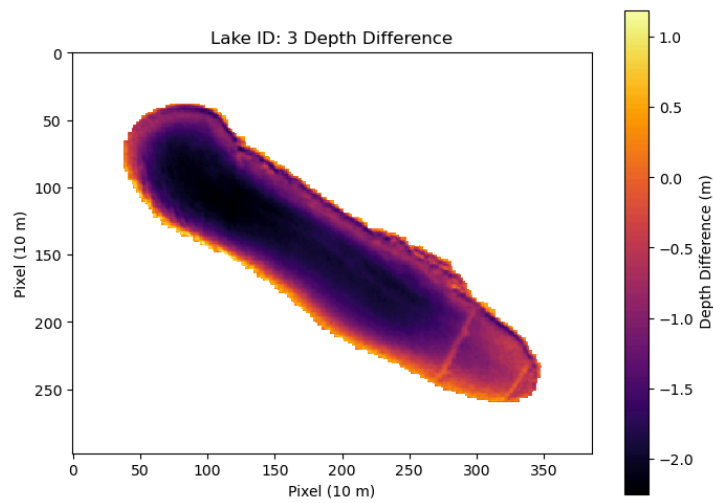*Figure 6.2 Lakes on SK, chosen for their varied surfaces.*

Figure 6.3. Lake 3 (79N) Depth Difference plot between ML-prediction and radiative transfer estimate
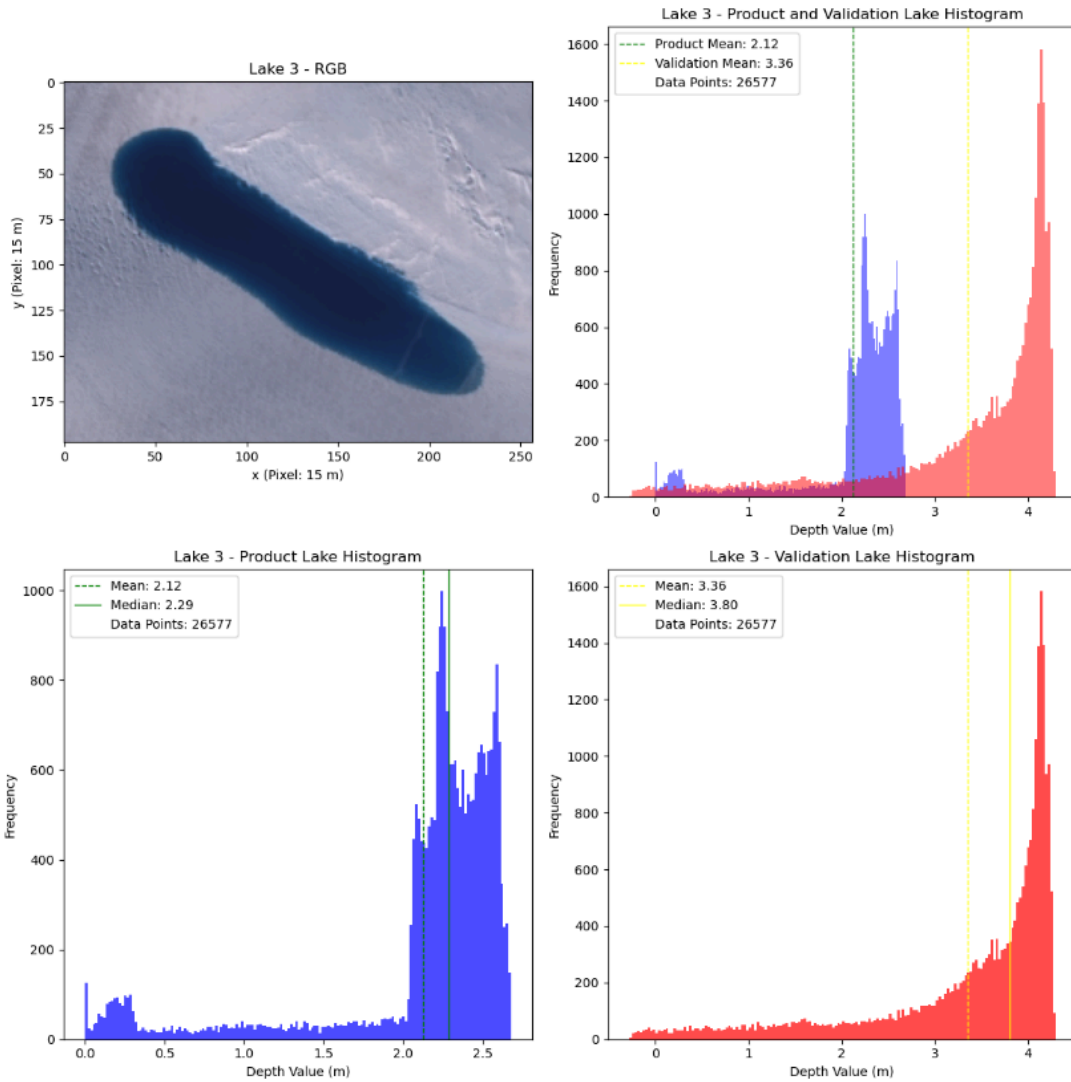
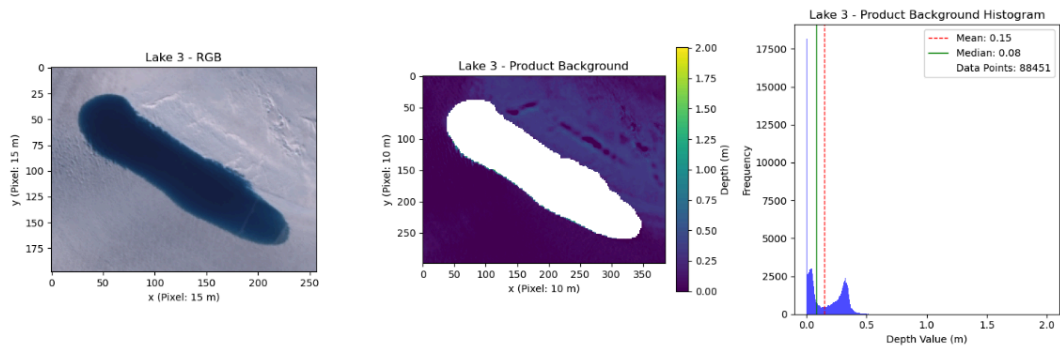Figure 6.4 Histogram of depth estimates of model vs radiative

Figure 6.5: Background analysis showing bias of model
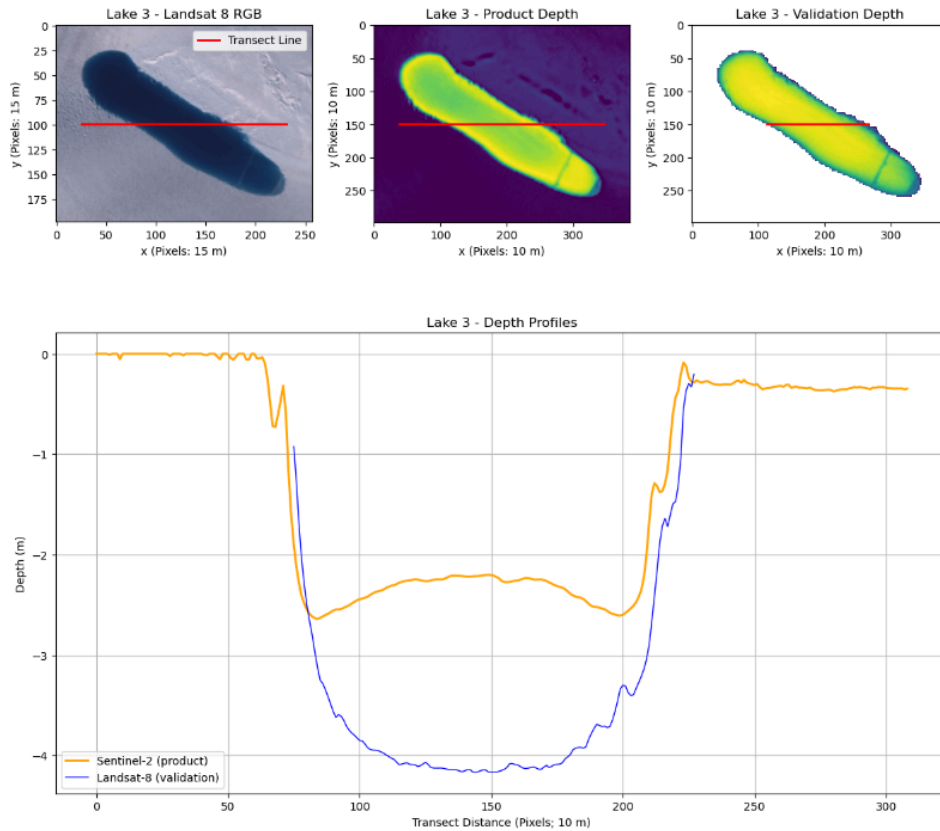
Figure 6.6 - Transection showing lake-bed bulge phenomenon

6.4   Recommendations for products improvement

The correspondence between SGL-volumes estimated from Landsat-8, and this ML-based variant reveals several areas of improvement. During validation we did not include a post-processing step, which could close false lid-predictions. There also appears to be a consistent underestimate of the actual depths, even when compared to known underestimates of the depths.

To resolve the lid-like artifacts predicted, a method of cut-mixing or cow-mixing has shown itself useful in related areas of study. These were not included in the present model used, as the depth-estimates were believed too sparse for performing such admixtures across samples of the data. A similar resolution could help with the mid-lake bulging phenomena, though in this case there is a much clearer need for expanding the available data.

A possible direction to improve upon the product would therefore be to invest more into both adding more depth-data for the SGLs on the GIS, as well as utilising a more iterative approach to extrapolating the available data. Examples here include the use of pseudo-labelling strategies, or using consistency based learning on the unlabelled portions of the depth data. Further development could see this turned from a currently less useful model of lake volumes into a somewhat reliable source of melt-water accretion estimates, which has a more significant downstream impact on the melt-cycles of the glacial interior.

7 References

Andrews, L. C. et al. (2018) Seasonal evolution of the subglacial hydrologic system modified by supraglacial lake drainage in Western Greenland. *Journal of Geophysical Research: Earth Surface* **123**, 1479-1496. 10.1029/2017JF004585

Blair, B. and Hofton, M.: IceBridge LVIS L2 Geolocated Surface Elevation Product. Boulder, Colorado USA: NASA DAAC at the National Snow and Ice Data Center. http://nsidc.org/data/docs/daac/icebridge/ilvis2/, 2012.

Brenner, A. C., Bindschadler, R. A., Thomas, R. H. and Zwally, H. J.: Slope-induced errors in radar altimetry over continental ice sheets, J. Geophys. Res. - Oceans, vol. 88, no.C3, pp. 1617–1623, 1983.

Das, S.B. et al. (2008) Fracture propagation to the base of the Greenland Ice Sheet during supraglacial lake drainage. *Science* **320**, 778-781. 10.1126/science.1153360

ENVEO, Greenland Ice Sheet Monthly Mass Flux Ice Discharge [v1] ,2014-2023, ESA, Greenland Ice Sheet CCI, 2024.

Fausto, R.S. and van As, D. 2019. Programme for monitoring of the Greenland ice sheet (PROMICE): Automatic weather station data. Version: v03, Dataset published via Geological Survey of Denmark and Greenland. doi: https://doi.org/10.22008/promice/data/aws

Fausto, R. S., van As, D., Mankoff, K. D., Vandecrux, B., Citterio, M., Ahlstrøm, A. P., Andersen, S. B., Colgan, W., Karlsson, N. B., Kjeldsen, K. K., Korsgaard, N. J., Larsen, S. H., Nielsen, S., Pedersen, A. Ø., Shields, C. L., Solgaard, A. M., and Box, J. E.: Programme for Monitoring of the Greenland Ice Sheet (PROMICE) automatic weather station data, Earth Syst. Sci. Data, 13, 3819–3845, https://doi.org/10.5194/essd-13-3819-2021 , 2021.

Forsberg, R., Sørensen, L. & Simonsen, S: Greenland and Antarctica Ice Sheet Mass Changes and Effects on Global Sea Level. Surveys in Geophysics (2017) 38: 89. doi:10.1007/s10712-016-9398-7

Geological Survey of Denmark and Greenland: PROMICE, Programme for Monitoring of the Greenland Ice Sheet. http://www.promice.org/home.html, 2015.

Groh, A.; Horwath, M.; Horvath, A.; Meister, R.; Sørensen, L.S.; Barletta, V.R.; Forsberg, R.; Wouters, B.; Ditmar, P.; Ran, J.; Klees, R.; Su, X.; Shang, K.; Guo, J.; Shum, C.K.; Schrama, E.; Shepherd, A. Evaluating GRACE Mass Change Time Series for the Antarctic and Greenland Ice Sheet—Methods and Results. Geosciences (2019), 9, 415. doi:10.3390/geosciences9100415.

Hoffman, M.J. et al. (2011) Links between acceleration, melting, and supraglacial lake drainage of the western Greenland Ice Sheet. *Journal of Geophysical Research: Earth Surface* **116**, F4, F04035. 10.1029/2010JF001934

Hvidberg, C.S., et al., User Requirements Document for the Ice_Sheets_cci project of ESA's Climate Change Initiative, version 1.5, 03 Aug 2012. Available from: http://www.esa-icesheets-cci.org/

Hvidberg, C. S., Grinsted, A., Dahl-Jensen, D., Khan, S. A., Kusk, A., Andersen, J. K., Neckel, N., Solgaard, A., Karlsson, N. B., Kjær, H. A., and Vallelonga, P., "Surface velocity of the Northeast Greenland Ice Stream (NEGIS): assessment of interior velocities derived from satellite data by GPS", The Cryosphere, 14, 3487–3502, https://doi.org/10.5194/tc-14-3487-2020, 2020.

Joughin, I. 2002. Ice-sheet velocity mapping: a combined interferometric and speckle-tracking approach. Annals of Glaciology, 34, 195–201. https://doi.org/10.3189/172756402781817978

Joughin, I., B. Smith, I. Howat, and T. Scambos. 2015, updated 2018. MEaSUREs Greenland Ice Sheet Velocity Map from InSAR Data, Version 2. [Indicate subset used]. Boulder, Colorado USA. NASA National Snow and Ice Data Center Distributed Active Archive Center. doi: https://doi.org/10.5067/OC7B04ZM9G6Q [Date Accessed: Date accessed: August 2020]

Joughin, I., I. Howat, B. Smith, and T. Scambos. 2020. MEaSUREs Greenland Ice Velocity: Selected Glacier Site Velocity Maps from InSAR, Version 3. [Indicate subset used]. Boulder, Colorado USA. NASA National Snow and Ice Data Center Distributed Active Archive Center. doi: https://doi.org/10.5067/YXMJRME5OUNC [Date accessed: August 2020]

Kappelsberger, M. T., Strößenreuther, U., Scheinert, M., Horwath, M., Groh, A., Knöfel, C., et al. (2021). Modeled and observed bedrock displacements in north-east Greenland using refined estimates of present-day ice-mass changes and densified GNSS measurements. Journal of Geophysical Research: Earth Surface, 126, e2020JF005860. https://doi.org/10.1029/2020JF005860

Khvorostovsky, K.: Merging and analysis of elevation time series over Greenland ice sheet from satellite radar altimetry, IEEE Trans. Geosc. Remote Sens., 50, 1:23–36.doi: 10.1109/TGRS.2011.2160071, 2012.

King, Michalea D., Howat, Ian M., Jeong, Seongsu, Noh, Myoung J., Wouters, Bert, Noël, Brice, van den Broeke, Michiel R.: Seasonal to decadal variability in ice discharge from the Greenland Ice Sheet , The Cryosphere 12(12), Copernicus GmbH, 3813–3825, 12 2018

King, Michalea D., Howat, Ian M., Candela, Salvatore G., Noh, Myoung J., Jeong, Seonsgu, Noël, Brice P. Y., van den Broeke, Michiel R., Wouters, Bert, Negrete, Adelaide: Dynamic ice loss from the Greenland Ice Sheet driven by sustained glacier retreat , Communications Earth & Environment 1(1), Springer Science and Business Media LLC, 8 2020

Krabill, W. B.: IceBridge Level-4 ATM Surface Elevation Rate of Change. Boulder, Colorado USA: NASA DAAC at the National Snow and Ice Data Center. http://nsidc.org/data/idhdt4.html, 2014.

Krabill, W. B.: IceBridge ATM L1B Elevation and Return Strength. Boulder, Colorado USA: NASA DAAC at the National Snow and Ice Data Center. http://nsidc.org/data/ilatm1b.html, 2010.

Krabill, W. B., Abdalati, W., Frederick, E., Manizade, S., Martin, C., Sonntag, J., Swift, R., Thomas, R. and J. Yungel, J.: Aircraft laser altimetry measurement of elevation changes of the Greenland Ice Sheet: technique and accuracy assessment, J. Geodyn., 34:357–376. doi: 10.1016/S0264-3707(02)00040-6, 2002.

Legresy, B., Papa, F., Remy, F., Vinay, G., van den Bosch, M. and Zanife, O.-Z.: ENVISAT radar altimeter measurements over continental surfaces and ice caps using the ICE-2 retracking algorithm, Remote Sens. Environ., 95(2):150–163. doi: 10.1016/j.rse.2004.11.018, 2005.

Liang, Y.-L. et al. (2012) A decadal investigation of supraglacial lakes in West Greenland using a fully automatic detection and tracking algorithm. *Remote Sensing of Environment* **123**, 127-138. 10.1016/j.rse.2012.03.020

McMillan, M., Muir, A., Shepherd, A., Escolà, R., Roca, M., Aublanc, J., Thibaut, P., Restano, M., Ambrozio, A., and Benveniste, J.: Sentinel-3 Delay-Doppler altimetry over Antarctica, The Cryosphere, 13, 709–722, https://doi.org/10.5194/tc-13-709-2019, 2019.

Mankoff, K., Solgaard, A., Larsen, S., 2020, "Greenland Ice Sheet solid ice discharge from 1986 through last month: Discharge", https://doi.org/10.22008/promice/data/ice_discharge/d/v02, GEUS Dataverse, V100

Mankoff, Kenneth D., Solgaard, Anne, Colgan, William, Ahlstrøm, Andreas P., Khan, Shfaqat Abbas, Fausto, Robert S.: Greenland Ice Sheet solid ice discharge from 1986 through March 2020 , Earth System Science Data 12(2), Copernicus GmbH, 1367–1383, 6 2020

Mouginot, Jérémie, Rignot, Eric, Bjørk, Anders A., van den Broeke, Michiel, Millan, Romain, Morlighem, Mathieu, Noël, Brice, Scheuchl, Bernd, Wood, Michael: Forty-six years of Greenland Ice Sheet mass balance from 1972 to 2018 , Proceedings of the National Academy of Sciences , Proceedings of the National Academy of Sciences, 201904242, 4 2019

Otosaka, I. N., Shepherd, A., Ivins, E. R. et al.: Mass balance of the Greenland and Antarctic ice sheets from 1992 to 2020, Earth Syst. Sci. Data, 15, 1597–1616, https://doi.org/10.5194/essd-15-1597-2023, 2023.

Philpot WD. Bathymetric mapping with passive multispectral imagery. Appl Opt. 1989 Apr 15;28(8):1569-78. doi: 10.1364/AO.28.001569. PMID: 20548701. https://doi.org/10.5194/tc-10-15-2016

Pope, A., Scambos, T. A., Moussavi, M., Tedesco, M., Willis, M., Shean, D., & Grigsby, S. (2016). Estimating supraglacial lake depth in West Greenland using Landsat 8 and comparison with other multispectral methods. *The Cryosphere, 10*(1), 15.

Rastner, P., Bolch, T., Mölg, N., Machguth, H., Le Bris, R., Paul, F. 2012, updated 2018. The first complete inventory of the local glaciers and ice caps on Greenland. The Cryosphere, 6, 1483-1495. doi:10.5194/tc-6-1483-2012

Roemer, S., Legresy, B., Horwath, M., and Dietrich, R.: Refined analysis of radar altimetry data applied to the region of the subglacial Lake Vostok/Antarctica, Remote Sens. Environ., vol. 106, no. 3, pp. 269–284, 2007.

Rowley, N.A. & Fegyveresi, J.M. (2019) Generating a supraglacial melt-lake inventory near Jakobshavn, West Greenland, using a new semi-automated lake-mapping technique. *Polar Geography* **42:2**, 89-108. 10.1080/1088937X.2019.1578289

Shepherd, A., Ivins, E. R., Geruo, A., Barletta, V. R., Bentley, M. J., Bettadpur, S., ... &Horwath, M. (2012). A reconciled estimate of ice-sheet mass balance. *Science*, *338*(6111), 1183-1189.

Shepherd, A., Ivins, E., Rignot, E. et al. Mass balance of the Antarctic Ice Sheet from 1992 to 2017. Nature 558, 219–222 (2018). https://doi.org/10.1038/s41586-018-0179-y

Shepherd, A., Ivins, E., Rignot, E. et al. Mass balance of the Greenland Ice Sheet from 1992 to 2018. Nature 579, 233–239 (2020). https://doi.org/10.1038/s41586-019-1855-2

Simonsen, S. B. and Sørensen, L. S. (2017): Implications of changing scattering properties on Greenland ice sheet volume change from Cryosat-2 altimetry. Remote Sensing of Environment, 190, p. 207-216, 2017.

Skourup, H., Barletta, V., Einarsson, I., Forsberg, R., Haas, C., Helm, V., Hendricks, S., Hvidegaard, S. M., and Sørensen, L. S.: ESA CryoVEx 2011: Airborne field campaign with ASIRAS radar, EM induction sounder and laser scanner. DTU Space, National Space Institute, Technical University of Denmark, 1st edition, 2011.

Slater T., A. Shepherd, M. Mcmillan, T. W. K. Armitage, I. Otosaka and R. J. Arthern, "Compensating Changes in the Penetration Depth of Pulse-Limited Radar Altimetry Over the Greenland Ice Sheet," in *IEEE Transactions on Geoscience and Remote Sensing*, vol. 57, no. 12, pp. 9633-9642, Dec. 2019, doi: 10.1109/TGRS.2019.2928232.

Smith, B., Sutterley, T., Dickinson, S., Jelley, B. P., Felikson, D., Neumann, T. A., Fricker, H. A., Gardner, A. S., Padman, L., Markus, T., Kurtz, N., Bhardwaj, S., Hancock, D. & Lee, J. (2022). ATLAS/ICESat-2 L3B Gridded Antarctic and Arctic Land Ice Height Change. (ATL15, Version 2). [Data Set]. Boulder, Colorado USA. NASA National Snow and Ice Data Center Distributed Active Archive Center. https://doi.org/10.5067/ATLAS/ATL15.002. [Greenland ice sheer subset used]. Date Accessed 12-05-2024.

Sneed, W.A. and Hamilton, G.S. (2007) Evolution of Melt Pond Volume on the Surface of the Greenland Ice Sheet. Geophysical Research Letters, 34. http://dx.doi.org/10.1029/2006GL028697

Solgaard, A., Kusk, A., Boncori, J. P. M., Dall, J., Mankoff, K. D., Ahlstrøm, A. P., Andersen, S. B., Citterio, M., Karlsson, N. B., Kjeldsen, K. K., Korsgaard, N. J., Larsen, S. H., & Fausto, R. S. (2021). Greenland ice velocity maps from the PROMICE project. Earth System Science Data, 13(7), 3491-3512. https://doi.org/10.5194/essd13-3491-2021

Sørensen, L. S., Simonsen, S. B., Forsberg, R., Stenseng, L., Skourup, H., Kristensen, S. S., & Colgan, W. (2017). Circum-Greenland, ice-thickness measurements collected during PROMICE airborne surveys in 2007, 2011 and 2015. Geological Survey of Denmark and Greenland Bulletin, 79-82.

Williamson, A.G. et al. (2017) A Fully Automated Supraglacial lake area and volume Tracking ("FAST") algorithm: Development and application using MODIS imagery of West Greenland. *Remote Sensing of Environment* **196**, 113-133. 10.1016/j.rse.2017.04.032

Yang, K. & Smith, L. (2013) Supraglacial streams on the Greenland Ice Sheet delineated from combined spectral-shape information in high-resolution satellite imagery. *IEEE Geosci. Remote Sens. Lett.,* 10 (4), 801- 805.

Yang, K. (2019) Supraglacial river and lake analysis [software]. *figshare.* 10.6084/m9.figshare.9758051.v1.

Zwally, H. Jay, Giovinetto, Mario B., Beckley, Matthew A., Saba, Jack L.: Antarctic and Greenland Drainage Systems, 2012, GSFC Cryospheric Sciences Laboratory